UNIVERSITY OF COPENHAGEN

Københavns Universitet

Structure elucidation of prenyl- and geranyl substituted coumarins in Gerbera piloselloides by NMR spectroscopy, electronic circular dichroism calculations, and single crystal X-ray crystallography

Li, Tuo; Ma, Xue; Fedotov, Daniil; Kjaerulff, Louise; Frydenvang, Karla Andrea; Coriani, Sonia; Hansen, Paul Robert; Kongstad, Kenneth Thermann; Stærk, Dan

Published in:
Molecules

DOI:
10.3390/molecules25071706

Publication date:
2020

Document version
Publisher's PDF, also known as Version of record

Document license:
CC BY

Citation for published version (APA):
Li, T., Ma, X., Fedotov, D., Kjaerulff, L., Frydenvang, K. A., Coriani, S., Hansen, P. R., Kongstad, K. T., & Stærk, D. (2020). Structure elucidation of prenyl- and geranyl substituted coumarins in *Gerbera piloselloides* by NMR spectroscopy, electronic circular dichroism calculations, and single crystal X-ray crystallography. *Molecules*, *25*, Article 1706. https://doi.org/10.3390/molecules25071706

Download date: 10. okt.. 2026

molecules

MDPI

Article

Structure Elucidation of Prenyl- and Geranyl-Substituted Coumarins in *Gerbera piloselloides* by NMR Spectroscopy, Electronic Circular Dichroism Calculations, and Single Crystal X-ray Crystallography

Tuo Li [1], Xue Ma [2], Daniil Fedotov [3], Louise Kjaerulff [1], Karla Frydenvang [1], Sonia Coriani [3], Paul Robert Hansen [1], Kenneth T. Kongstad [1] and Dan Staerk [1,*]

1 Department of Drug Design and Pharmacology, Faculty of Health and Medical Sciences, University of Copenhagen, Universitetsparken 2, DK-2100 Copenhagen, Denmark; tuo.li@siat.ac.cn (T.L.); louisek@sund.ku.dk (L.K.); karla.frydenvang@sund.ku.dk (K.F.); prh@sund.ku.dk (P.R.H.); kenneth.kongstad@sund.ku.dk (K.T.K.)

2 Engineering Research Center for the Development and Application of Ethnic Medicine and TCM, Guizhou Medical University, No.4 Beijing Road, Yunyan District, Guiyang 550004, China; xuema0111@163.com

3 Department of Chemistry, Technical University of Denmark, Kemitorvet Building 207, DK-2800 Kgs. Lyngby, Denmark; feniil@kemi.dtu.dk (D.F.); soco@kemi.dtu.dk (S.C.)

* Correspondence: ds@sund.ku.dk; Tel.: +45-35336177

Received: 18 February 2020; Accepted: 2 April 2020; Published: 8 April 2020

Abstract: Crude ethyl acetate extract of *Gerbera piloselloides* (L.) Cass. was investigated by dual high-resolution PTP1B/α-glucosidase inhibition profiling and LC-PDA-HRMS. This indicated the presence of a series of unprecedented prenyl- and geranyl-substituted coumarin derivatives correlated with both α-glucosidase and PTP1B inhibitory activity. Repeated chromatographic separation targeting these compounds led to the isolation of 13 new compounds, of which ten could be isolated as both enantiomers after chiral separation. The structures of all isolated compounds were characterized by HRMS and extensive 1D and 2D NMR analysis. The absolute configurations of the isolated compounds were determined by comparison of experimental and calculated electronic circular dichroism spectra. Compound **6** features a rare furan-oxepane 5/7 ring system, possibly formed through addition of a geranyl unit to C-3 of 5-methylcoumarin, representing a new type of geranyl-substituted coumarin skeleton. Compounds **19** and **24** are the first examples of dimeric natural products consisting of both coumarin and chromone moieties.

Keywords: *Gerbera piloselloides*; coumaroyl derivative; protein-tyrosine phosphatase 1B; α-glucosidase; chiral separation; electronic circular dichroism; X-ray

1. Introduction

Diabetes mellitus is a multifactorial disease characterized by insufficient regulation of glucose metabolism, with severe long-term micro- and macrovascular complications such as retinopathy, neuropathy, nephropathy and cardiovascular diseases. More than 463 million people were affected by diabetes worldwide in 2019, and this figure is estimated to increase to 700 million by 2045 [1]. Type 2 diabetes (T2D) comprises more than 90% of all diabetes cases and is characterized by decreased insulin sensitivity in target organs like muscle and adipose tissue as well as reduced pancreatic insulin secretion [2,3]. Thus, management of a relatively stable blood glucose in the interval 5–10 mmol/L

by hypoglycemic drugs is of utmost importance for diabetics. One target for management of T2D is protein tyrosine phosphatase 1B (PTP1B) [4,5], which acts as a negative modulator of insulin by dephosphorylation of the insulin receptor and the insulin receptor substrate. α-Glucosidase constitutes another potential T2D target enzyme [6]. It is found in the brush border of the small intestines, where it hydrolyses terminal non-reducing 1,4-linked α-glucose residues to absorbable monosaccharides for managing a low and stable blood glucose level. There are still no clinically approved PTP1B inhibitors for diabetics, and the clinically approved drugs acarbose, miglitol and voglibose are associated with side effects such as flatulence, diarrhea and stomach ache [7]. Thus, there is an unmet need for new PTP1B and α-glucosidase inhibitors as potential T2D drug leads.

Gerbera piloselloides (L.) Cass. (Compositae) is a perennial herb commonly found in southwest China. It is mentioned in local traditional medicine books, where it is recommended as a remedy for treating fever, cough, and snake bites [8]. Previous studies have shown that *Gerbera* spp. are rich in coumarins [9–16], with substituents regularly occurring at C-3 and C-4 of the α-pyrone moiety, as seen for dibothrioclinin I and II [11], gerdelavin A [12], and gerberlin A-C [13]. Coumarins from *Gerbera* have been reported to possess anticancer [13–15], antioxidant [16], antimicrobial [15], anti-HIV [17], and hypoglycemic activity [18]. However, to date only a few studies of the phytochemistry and the pharmacological activity of *G. piloselloides* and its constituents have been published [11,16,19], and this species therefore holds promise for discovery of new natural products with pharmacological activity.

The ability to pinpoint the constituent(s) correlated with one or more bioactivities in a complex extract can significantly speed up the identification of bioactive natural products. One way of achieving this is by microfractionation of the eluate from analytical-scale HPLC separation of crude extracts followed by assaying of the material in each well with selected assay(s). The results expressed as percentage inhibition are then plotted at their respective retention time to provide a high-resolution inhibition profile (biochromatogram) with a typical resolution of 4 to 10 datapoints per min. The biochromatogram can be represented underneath the chromatographic traces, which allows direct pinpointing of HPLC peaks correlated with peaks in the biochromatogram. This approach has been successfully used to accelerate identification of α-glucosidase [20], α-amylase [21], aldose reductase [22], and PTP1B [23] inhibitors as well as radical scavengers [24], using either single [25], dual [26], triple [22], or quadruple [27] high-resolution inhibition profiling.

Here, we report the combined use of LC-PDA-HRMS and dual high-resolution PTP1B/α-glucosidase inhibition profiling, that for the first time directly pinpoints α-glucosidase and PTP1B inhibitors in *G. piloselloides*. This was used to guide isolation towards a series of unusual prenyl- and geranyl-substituted coumarin derivatives with hitherto unprecedented skeletons - including dimeric coumarin derivatives formed by Diels-Alder cycloadditions. Full structure elucidation by 2D NMR spectroscopy and assignment of absolute configuration by electronic circular dichroism spectroscopy of these complex natural products provide important reference data for future studies of related structures.

2. Results

Crude ethyl acetate extract of *Gerbera piloselloides* showed moderate inhibition of PTP1B and α-glucosidase with IC_{50} values of 82.8 ± 0.96 μg/mL and 35.9 ± 0.03 μg/mL, respectively. Thus, two repeated analytical-scale HPLC separations were microfractionated into two 96-well microplates each, which after evaporation of the solvent and assaying using PTP1B and α-glucosidase, resulted in the dual high-resolution PTP1B/α-glucosidase inhibition profile (biochromatogram) shown in Figure 1.

The biochromatogram shows that constituents in peaks *7* and *13–27* are correlated with both PTP1B and α-glucosidase inhibitory activity. LC-HRMS analysis of the material eluted in the regions marked fraction F1 (dark green) and F2 (orange) implied that most of the constituents eluting in these regions have the same molecular formula $C_{20}H_{22}O_3$. However, the material eluted with Fraction 1 did not show correlation with inhibitory activity in the biochromatogram. To compare active and non-active compounds with the same molecular formula, Fraction 1 and 2 were selected for further investigation together with the constituents eluted with peaks *1–27*.

Material eluted with peaks *1-27* and fractions 1 and 2 were collected manually by preparative-scale HPLC. Fraction 2 was subsequently separated using an analytical-scale pentafluorophenyl (PFP) HPLC column, and two successive separations were microfractionated. The dual high-resolution inhibition profile of F2 is shown in Figure 2. This shows that the constituents eluting as peaks *13*, *14* and *16–21* are correlated with α-glucosidase and/or PTP1B inhibitory activity. Thus, the extract seems to contain multiple new compounds correlated with inhibitory activity towards both PTP1B and α-glucosidase - one of many unique features of natural products.

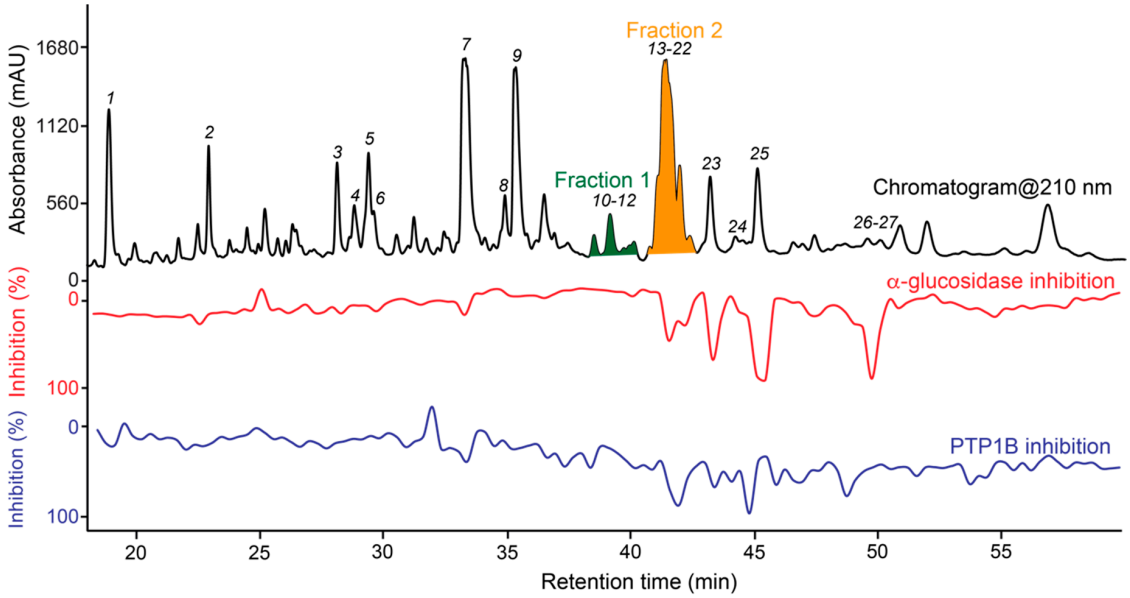

Figure 1. Dual high-resolution PTP1B/α-glucosidase inhibition profile of the crude ethyl acetate extract of *Gerbera piloselloides* shown with the UV chromatogram at 210 nm.

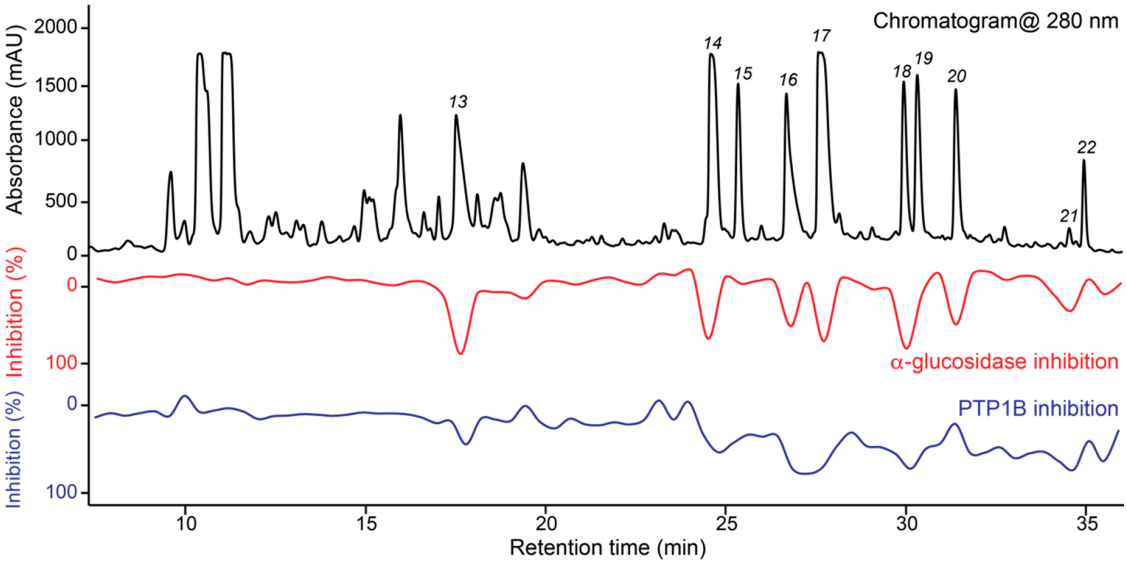

Figure 2. Dual high-resolution PTP1B/α-glucosidase inhibition profile of Fraction 2 of *Gerbera piloselloides* shown with the UV chromatogram at 280 nm.

Structure Elucidation of Prenyl- and Geranyl Coumarin Derivatives

Based on information from the two biochromatograms shown in Figures 1 and 2, material correlated with bioactivity as well as material suggested by LC-PDA-HRMS to be prenyl- or geranyl coumarin derivatives were isolated by preparative-scale HPLC followed

by analytical-scale HPLC as detailed in the Materials and Methods section. This led to isolation of the new compounds **2**, **5**, **6**, **8**, **10**, **11**, **14**, **15**, **17–19**, and **23–25** as well as identification of the known compounds marmesin (**1**) [28], 7-demethylsuberosin (**3**) [29], apigravin (**4**) [30], bothrioclinin (**7**) [31], (+)-2-[(2*R*)-6-acetyl-2,3-dihydro-5-hydroxybenzofuran-2-yl]- prop-2-enyl 15-methylbutanoate (**8**) [29], 3,5-bis-(isopent-2-en-1-yl)-4-hydroxyacetophenone (**9**) [32], 6-acetyl-2,2-dimethyl-8-(3-methylbut-2-en-1-yl)-2*H*-chromene (**12**) [33], and mutisicoumarin B (**16**) [34] by comparison of their ^{1}H NMR data with data from the literature. Retention times, HRESIMS, and ^{1}H NMR data for **1**, **3**, **4**, **7–9**, and **12** are given in Table S1, Supplementary Material.

Compound **2** showed a $[M + H]^+$ ion with *m/z* 277.1083 ($C_{15}H_{17}O_5^+$, ΔM −4.5 ppm), which suggests the molecular formula $C_{15}H_{16}O_5$. The ^{1}H NMR spectrum shows characteristic signals for a 1,2,3-trisubstituted benzene ring δ 7.12 (d, 7.4 Hz, H-6), δ 7.45 (dd, 8.3, 7.4 Hz, H-7) and δ 7.19 (d, 8.3 Hz, H-8)), two methyl singlets (δ 1.52, CH_3-13 and δ 1.57, CH_3-14) with HMBC correlations to C-4 (δ 163.7) and C-11 (δ 83.1), a methyl singlet (δ 2.72 CH_3-12) with HMBC correlations to C-4a (δ 115.5), C-5 (δ 139.0), and C-6 (δ 128.9), and two oxymethine signals at δ 4.58 (d, 4.1 Hz, H-9) and δ 3.75 (d, 4.1 Hz, H-10) with HMBC correlations to C-3 (δ 101.8) and C-2 (δ 164.7).

This suggested **2** to be the 9,10-dihydroxylated analogue of bothrioclinin (**7**) (Figure 3), and COSY, ROESY, HSQC and HMBC correlations, of which selected correlations are shown in Figure 4, confirmed this and allowed the full assignment of ^{1}H and ^{13}C NMR signals provided in Tables 1 and 2. The relative configuration of **2** was established to be 9*S**,10*S** based on the coupling constant (^3J = 4.1 Hz) between H-9 and H-10, which suggests a *cis* configuration as also reported for *cis*-khellactone [35]. Finally, the absolute configuration of **2** was assigned 9*S*,10*S* by comparing the ECD spectrum of **2** (Figure S8, Supplementary Material) with ECD data of *cis*-khellactone [35]. Compound **2** is a new compound for which the name gerbeloid 1 is proposed.

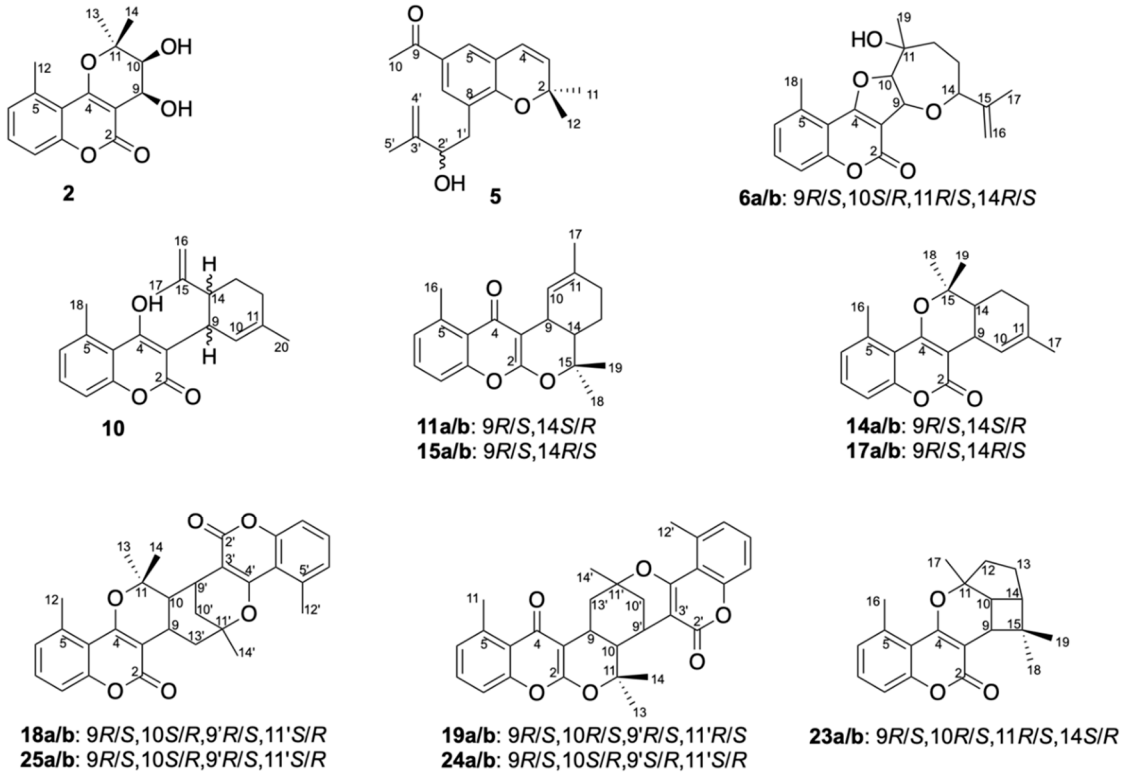

Figure 3. New prenyl- and geranyl coumarin derivatives **2**, **5**, **6**, **8**, **10**, **11**, **14**, **15**, **17-19** and **23–25** identified in the crude extract of *Gerbera piloselloides*.

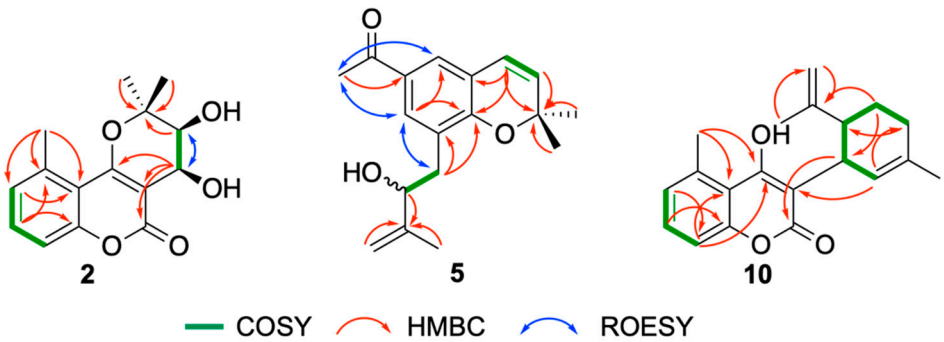

Figure 4. Selected COSY, ROESY and HMBC correlations of compounds **2**, **5**, and **10**.

Table 1. ^{1}H NMR (600 MHz) Spectroscopic Data of **2**, **5**, **6**, and **10** [a].

Pos.	δ_H (*J*, in Hz)			Pos.	δ_H (*J*, in Hz)
	2	**6**	**10**		**5**
6	7.12, d (7.4 Hz)	7.26, d (8.4 Hz)	6.99, d (7.5 Hz)	3	5.76, d (9.8 Hz)
7	7.45, dd (8.3, 7.4 Hz)	7.56, dd (8.4, 7.5 Hz)	7.29, dd (8.3, 7.5 Hz)	4	6.42, d (9.8 Hz)
8	7.19, d (8.3 Hz)	7.20, d (7.5 Hz)	7.03, d (8.3 Hz)	5	7.56, d (2.1 Hz)
9	4.58, d (4.1 Hz)	5.51, d (7.6 Hz)	3.83, d (10.5 Hz)	7	7.70, d (2.1 Hz)
10	3.75, d (4.1 Hz)	4.78, d (7.6 Hz)	5.32, br s	10	2.52, s
11				11	1.46, s
12	2.72, s	1.98, ddd (14, 13.0, 3.3 Hz); 1.80, m	2.25, m2.02, m	12	1.47, s
13	1.52, s	2.00, m; 1.68, m	1.77, m	1′	2.95, dd (13.3, 5.5 Hz); 2.68, dd (13.4, 7.8 Hz)
14	1.57, s	3.52, d (10.0 Hz)	2.96, br s	2′	4.31, dd (7.4, 5.7 Hz)
16		4.73[b]; 4.81[b]	4.52, s; 4.54, s	4′	4.76[b]; 4.83 [b]
17		1.66, s	1.68, s	5′	1.81, s
18		2.72, s	2.76, s		
19		1.58, s	1.70, s		

[a] NMR data obtained with samples in methanol-d_4. [b] Signals overlapping with residual solvent signal of methanol at δ 3.31, water at δ 4.87 or other signals from the molecule.

Table 2. ^{13}C NMR (150 MHz) Spectroscopic Data of **2**, **5**, **6**, **10**, **11**, **14**, **15**, **17**, and **23** [a].

Pos.	δ_C								Pos.	δ_C
	2	**6**	**10**	**11**	**14**	**15**	**17**	**23**		**5**
2	164.7	161.4	165.5	162.6	164.1	162.7	163.9	165.2	2	78.9
3	101.8	102.7	106.4	100.5	102.9	99.7	102.9	103.9	3	132.0
4	163.7	171.1	171.4	182.2	162.4	181.8	163.5	163.6	4	122.8
4a	115.5	112.2	118.6	122.3	120	121	116.1	116.1	4a	121.7
5	139.0	138.5	138.8	133.0	138.0	141.3	138.2	138.1	5	126.4
6	128.9	115.5	127.6	133.1	128.2	128.9	128.7	128.9	6	130.7
7	132.8	133.8	130.7	128.9	131.6	133.0	132.0	132.1	7	133.1
8	115.9	127.5	115.1	116.2	115.4	116.3	115.7	115.9	8	127.7
8a	155.5	157.9	155.2	155.7	154.9	155.8	155.0	155.0	8a	156.8
9	66.5	76.1	37.3	31.1	31.7	33.7	34.1	37.4	9	199.6
10	73.8	95.9	126.0	121.7	121.0	123.1	122.8	38.4	10	26.1
11	83.1	74.0	135.5	135.4	135.2	134.7	135.2	88.2	11	28.6
12	23.3	36.1	31.4	30.5	30.3	32.2	32.0	40.6	12	28.6
13	24.4	29.9	30.3	21.4	21.2	25.4	25.5	26.6	1′	36.8
14	22.9	78.3	45.4	41.0	40.3	47.1	46.2	48	2′	75.8
15		147.5	150	84.8	83.6	86.4	86.3	40.4	3′	148.6
16		111.0	110.6	22.4	23.3	22.6	23.9	23.4	4′	111.1
17		19.5	19.2	23.4	23.4	23.3	23.4	27.6	5′	17.7
18		21.1	23.2	25.5	25.6	27.1	27.3	34.1		
19		30.8	23.4	25.4	25.0	20.1	20.3	17.9		

[a] NMR data obtained with samples in methanol-d_4.

Compound **5** showed a $[M + H]^+$ ion with *m/z* 287.1637 ($C_{18}H_{23}O_3^+$, ΔM 1.6 ppm), which suggests the molecular formula $C_{18}H_{22}O_3$. The ^{1}H NMR spectrum of **5** displays characteristic signals for the *cis*-coupled H-3 (δ 5.74, d, 9.8 Hz) and H-4 (δ 6.42, d, 9.8 Hz), the *meta*-coupled H-5 (δ 7.56, d, 2.1 Hz) and H-7 (δ 7.70, d, 2.1 Hz), a methyl signal for CH_3-10 (δ 2.52, s), and two methyl singlets for CH_3-11 (δ 1.46, s) and CH_3-12 (δ 1.47, s). This confirms that **5** possesses a 2,2-dimethyl-2*H*-chromene core skeleton with an acetyl at C-6 and a second substituent at C-8, which based on the residual molecular formulas, is in agreement with a hydroxyisoprenyl unit (C_5H_9O). The COSY spectrum revealed a CH_2-CH-O spin system, and HMBC correlations from H-1′ to C-8′ and C-8a′ as well as from H-2′, H-4′ and H-5′ to C-3′ confirmed a 2-hydroxy-3-methylbut-3-en-1-yl unit at C-8. Compound **5** gradually degraded in solution, and it was therefore not possible to determine the absolute configuration at C-2′. The structure of **5** is shown in Figure 3, selected COSY, ROESY and HMBC correlations are shown in Figure 4, ^{1}H NMR, COSY, ROESY, HSQC and HMBC spectra are provided in Figures S33–S38, Supplementary Material, and fully assigned ^{1}H and ^{13}C NMR data are provided in Tables 1 and 2. Compound **5** is a new compound for which the name gerbeloid 2 is proposed.

Compound **6** showed a $[M + H]^+$ ion with *m/z* 343.1527 ($C_{20}H_{23}O_5^+$, ΔM 3.8 ppm) and a $[M + Na]^+$ ion with *m/z* 365.1359 ($C_{20}H_{22}O_5Na^+$, ΔM 0.1), which suggested the molecular formula $C_{20}H_{22}O_5$ with a hydrogen deficiency index of 10. The ^{1}H NMR spectrum of **6** shows characteristic signals of a 5-methylcoumarin moiety substituted at C-3 and C-4 (δ 7.26 (d, 8.4 Hz, H-6), δ 7.56 (dd, 8.4, 7.5 Hz, H-7), δ 7.20 (d, 7.5 Hz, H-8), and δ 2.71 (s, CH_3-18)) as also seen for **2** and **7**, *vide supra*; leaving a residual molecular formula of $C_{10}H_{16}O_3$ and three hydrogen deficiency index numbers for the substituents at C-3 and C-4. COSY correlations were observed between oxymethines H-9 ↔ H-10 and between H-12 ↔ H-13 ↔ H-14, and with HMBC correlations from H-9 to C-14 and from H-14 to C-9 as well as from H-10 and H-12 to the oxymethine C-11, this established the oxepane ring.

Furthermore, the prop-1-en-2-yl unit at C-14 was established by HMBC correlations from H-14 to C-15, C-16 and C-17, and the methyl group at C-11 was established by HMBC correlations from H-19 to C-11. Finally, the ether linkage between C-4 and C-10 to form the 2,3-dihydrofuran moiety was inferred from the downfield shift of C-4 (δ 171.0) in **6** compared to **2** (δ 164.7) and **7** (δ 161.6), as also reported by Qiang and co-workers for gerbelin 3 [13], as well as the need to establish a ring closure as determined from the hydrogen deficiency index. Thus, the structure of **6** contains a rare furan-oxepane 5/7 ring system formed by a geranyl unit.

The relative configuration 9*R**,10*S**,11*R**,14*R** was established based on the *cis* coupling constants between H-9 and H-10 (^3J = 7.6 Hz) as well as the ROESY correlations H-9 ↔ H-14, and between H-10 ↔ CH_3-19 (Figure 5A). An ECD spectrum of **6** indicated the material to be an enantiomeric mixture, and subsequent chiral separation showed two enantiomers (**6a** and **6b**) in a 1:1 ratio (Figure 5B). The two enantiomers were isolated, and their experimental ECD spectra (Figure 5D) were as expected completely opposite. After a conformational search, the 10 lowest-energy conformations of **6a** were obtained by energy minimization at the B3LYP/6-311G(d,p) level in CH_3CN (Figure S4 and Tables S2 and S3, Supplementary Material) and their ECD spectra calculated. The total Boltzmann-averaged ECD spectrum is shown in Figure 5D, confirming **6a** to be 9*R*,10*S*,11*R*,14*R* and **6b** to be 9*S*,10*R*,11*S*,14*S*. (Figure 5C), with an enantiomeric similarity index (Δ_{ESI}) of 0.80. Selected COSY, ROESY and HMBC correlations are shown in Figure 5A, ^{1}H NMR, COSY, ROESY, HSQC and HMBC spectra are provided in Figures S39–S44, Supplementary Material, and fully assigned ^{1}H and ^{13}C NMR data are provided in Tables 1 and 2. Compounds **6a** and **6b** are new compounds for which the names gerbeloid 3a and gerbeloid 3b are proposed.

Compound **8** showed a $[M + H]^+$ ion with *m/z* 319.1535 ($C_{18}H_{23}O_5^+$, ΔM 1.6 ppm), which suggested the molecular formula $C_{18}H_{22}O_5$ with a hydrogen deficiency index of 8. The ^{1}H NMR data of **8** are almost identical with data reported for 2-[(2*S**)-6-acetyl-2,3-dihydro-5-hydroxybenzofuran-2-yl]prop-2-enyl 3-methylbutanoate [29,36]. There is no optical rotation reported for this compound, but the optical rotation $[\alpha]^{25}{}_D$ + 60.8 (*c* 7.2 mM MeOH) of **8** has the opposite sign as the closely reported compounds (−)-2*S*-6,12-dihydroxytremetone and (−)-(*S*)-2-(5-acetyl-6-hydroxy-2,3-dihydrobenzofuran-2-yl)allyl

isobutyrate [37]. Furthermore, the experimental ECD spectrum of **8** shows positive Cotton effects around 195 and 265 nm and a negative Cotton effect around 225 nm (Figure S8, Supplementary Material), whereas the experimental and calculated ECD spectra of (−)-2*S*-6,12-dihydroxytremetone show negative Cotton effects around 205 and 280 nm and a positive Cotton effect around 240 nm [37].

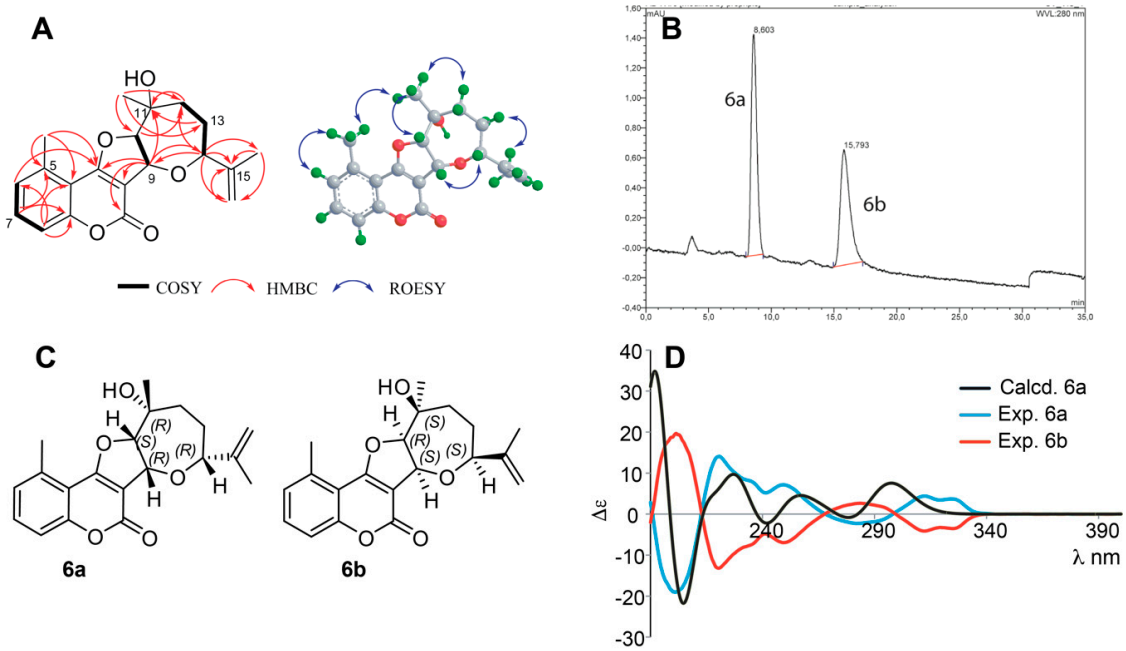

Figure 5. (**A**): Key 2D NMR correlations of **6**. (**B**): Chiral separation of 6 showing two enantiomers in a 1:1 ratio. (**C**): structures of **6a** and **6b** with the absolute configuration of stereocenters. (**D**): Calculated ECD spectrum of **6a** and experimental ECD spectra of **6a** and **6b**.

Thus, **8** is tentatively assigned the *R* configuration at C-2, and 2-[(2*S**)-6-acetyl-2,3-dihydro-5-hydroxybenzofuran-2-yl]prop-2-enyl 3-methylbutanoate, previously isolated from the closely related *Leibnitzia anandria* Sch. Bip. [36] and *Gerbera saxatilis* [29], should most likely also be assigned the *R* configuration at C-2 based on biosynthetic arguments. Full assignment of the HRMS and ^{1}H NMR data are included in Table S1, Supplementary Material, and ^{1}H NMR, COSY, ROESY, HSQC and HMBC spectra are provided in Figures S48–S52, Supplementary Material.

HRESIMS data for the material eluted with peaks *10–11*, *14–15* and *17* showed $[M + H]^+$ ions suggesting that these compounds all have the formula $C_{20}H_{22}O_3$. The 1D and 2D NMR spectra of **14** and **17** (Figures S72–S77 and Figures S88–S93, Supplementary Material) suggest structures consisting of the same 5-methylcoumarin moiety substituted at C-3 and C-4 as seen in **2**, **6** and **7**. Furthermore, detailed analysis of the NMR spectra suggested **14** and **17** to contain the same pyrano[3,2-*c*]coumarin core skeleton that was obtained as product of the microwave-accelerated domino Knoevenagel hetero Diels-Alder reaction between 4-hydroxycoumarin and citronellal [38], but with a methyl group at C-5 and a double bond between C-10 and C-11 (Figure 3).

HMBC and COSY correlations support the structures of **14** and **17**, with HMBC correlations from H-18 to C-4, from H-9 to the carbonylic C-2 and the olefinic C-3, and from H-14 to the oxygenated C-15 confirming the pyrano[3,2-*c*]coumarin skeleton (Figure 6). Compounds **14** and **17** are diastereomers, and the vicinal coupling $^{3}J_{H9,H14}$ = 6.8 Hz for **14** and a ROESY correlation between H-9 and H-14, support these two protons to be *cis* in **14**; whereas the vicinal coupling $^{3}J_{H9,H14}$ = 10.9 Hz for **17** as well as ROESY correlations between H-9 and CH_3-18 and between H-14 and CH_3-19 support these two protons to be *trans* in **17**. Both **14** and **17** are racemic mixtures, as seen from the 1:1 peak ratio upon chiral separation (Figures S1 and S2, Supplementary Material), and separation of the two enantiomers allowed comparison of their experimental and calculated ECD spectra. The absolute

configurations are therefore assigned 9*R*,14*S* for **14a** and 9*S*,14*R* for **14b** (with Δ_{ESI} of 0.94), and 9*R*,14*R* for **17a** and 9*S*,14*S* for **17b** (with Δ_{ESI} of 0.86), as depicted in Figure 6. ^{1}H NMR, COSY, ROESY, HSQC and HMBC spectra are provided in Figures S72–S77 and Figures S88–S93, Supplementary Material, and fully assigned ^{1}H and ^{13}C NMR data are provided in Tables 2 and 3. Compounds **14a**/**b** and **17a**/**b** are new compounds for which the names gerbeloid 6a/gerbeloid 6b and gerbeloid 8a/gerbeloid 8b, respectively, are proposed.

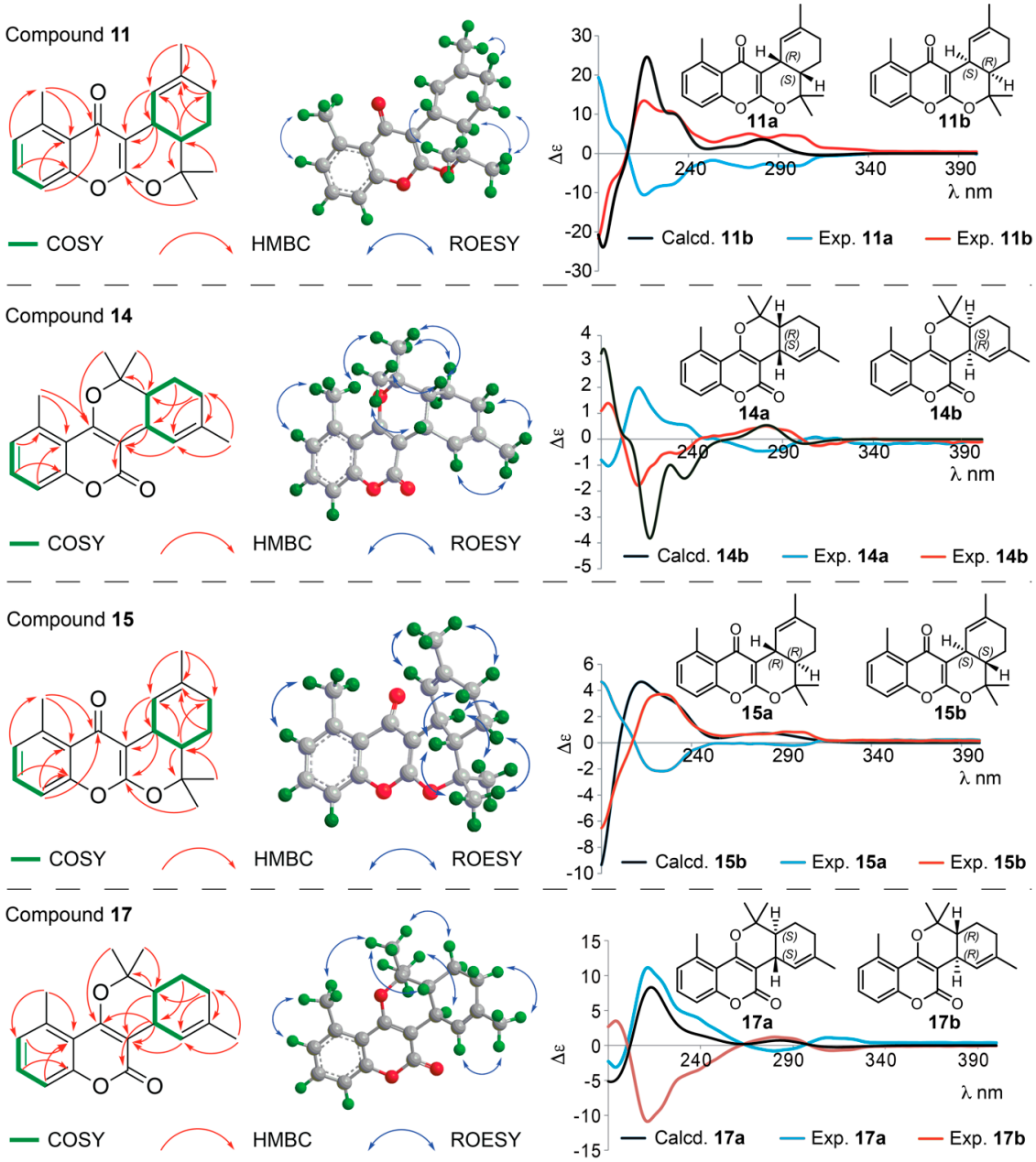

Figure 6. Left: Key COSY and HMBC correlations of **11**, **14**, **15** and **17**. **Middle**: Key ROESY correlations to establish relative configuration of one of the enantiomers of **11**, **14**, **15** and **17**. **Right**: Calculated ECD spectra of **11b**, **14b**, **15b** and **17a** and experimental ECD spectra of the enantiomers **11a/b**, **14a/b**, **15a/b** and **17a/b**. The enantiomeric structures of **11**, **14**, **15** and **17** shown with absolute configuration of the stereocenters determined based on the ECD data.

Table 3. ^{1}H NMR (600 MHz) Spectroscopic Data of **11**, **14**, **15**, **17**, and **23** [a].

Pos.	11	14	15	17	23
6	7.13, d (7.3 Hz)	7.08, d (7.4 Hz)	7.14, d (7.5 Hz)	7.08, d (7.5 Hz)	7.11, d (7.5 Hz)
7	7.47, dd (8.3, 7.3 Hz)	7.39, dd (8.2, 7.4 Hz)	7.48, dd (8.3, 7.5 Hz)	7.39, dd (8.3, 7.5 Hz)	7.41, dd (8.4, 7.5 Hz)
8	7.22, d (8.3 Hz)	7.13, d (8.2 Hz)	7.23, d (8.3 Hz)	7.13, d (8.3 Hz)	7.16, d (8.3 Hz)
9	3.51, dd (6.7, 4.0 Hz)	3.42, dd (6.8, 5.4 Hz)	3.21, d (10.8 Hz)	3.11, d (10.9 Hz)	3.01, d (9.4 Hz)
10	6.25, br s	6.18, br s	6.24, m	6.24, m	2.72 (m)
12	2.02, m; 1.98, m	2.06, m; 1.98, m	2.19, br s	2.19, m	1.91, dd (13.0, 7.5 Hz); 2.07, dd (12.8, 7.5 Hz)
13	2.04, m; 1.38, m	2.02, m; 1.34, m	1.96, m; 1.49, m	1.98, m; 1.47, m	1.76, dd (14.0, 7.5 Hz); 1.73, m
14	1.88, ddd (11.5, 6.1, 3.0 Hz)	1.88, ddd (11.8, 6.3, 3.0 Hz)	1.7, ddd (13.0, 10.8, 2.1 Hz)	1.71, ddd (12.7, 11.0, 2.0 Hz)	2.50, dd (8.1, 7.0 Hz)
16	2.80, s	2.69, s	2.81, s	2.70, s	2.74, s
17	1.67, s	1.68, s	1.68, s	1.68, s	1.56, s
18	1.51, s	1.57, s	1.54, s	1.61, s	1.40, s
19	1.42, s	1.41, s	1.26, s	1.26, s	0.88, s

[a] NMR data obtained with samples in methanol-d_4.

Synthesis of the pyrano[3,2-*c*]coumarin core skeleton via the microwave-accelerated domino Knoevenagel hetero Diels-Alder reaction between 4-hydroxycoumarin and citronellal [38], also provided products with the pyrano[2,3-*b*]chromen-4-one core skeleton. This is because the final cyclisation of the chromane-2,4-dione intermediate can occur via two different 4 + 2 cycloadditions, and one can predict that the potential geran-1-ylidene-chromane-2,4-dione intermediate for biosynthesis of **14** and **17** (lactones) could also lead to formation of the isomeric keto products with the pyrano[2,3-*b*]chromen-4-one core skeleton (Scheme S1, Supplementary Material). The ^{13}C NMR carbonyl resonances for C-4 in both **11** and **15** in fact suggest that the two compounds are chromone (keto) products, where C-4 is at δ 182.2 in **11** and δ 181.8 in **15** (Table 2). Additionally, HMBC correlations from CH_3-18 and H-9 to C-2, from H-9 and H-10 to C-3 and from H-8 and CH_3-16 to C-4 in both compounds support the pyrano[2,3-*b*]chromen-4-one core skeleton (Figure 6). Key COSY and HMBC correlations used for structure elucidation of **11** and **15** are shown in Figure 6. The relative configurations of **11** (9*R**,14*S**) and **15** (9*R**,14*R**) were established based on the vicinal coupling between H-9 and H-14 ($^{3}J_{H9,H14}$ = 6.7 Hz *cis* in **11** and $^{3}J_{H9,H14}$ = 10.8 Hz *trans* in **15**) (Tables 2 and 3) and ROESY correlations (Figure 6), showing that **11** and **15** are diastereomers. By chiral resolution, two enantiomeric pairs **11a**/**b** of **11** and **15a**/**b** of **15** were obtained in a 1:1 ratio (Figure S1, Supplementary Material), and ECD spectra were measured of each of the separated enantiomers. Comparison of the experimental and calculated ECD spectra (Figure 6) allowed assignment of the absolute configurations to be 9*R*,14*S* for **11a** and 9*S*,14*R* for **11b** (with Δ_{ESI} of 0.98), and 9*R*,14*R* for **15a** and 9*S*,14*S* for **15b** (with Δ_{ESI} of 0.95). ^{1}H NMR, COSY, ROESY, HSQC and HMBC spectra of **11** and **15** are provided in Figures S61–S66 and Figures S78–S83, Supplementary Material, and ^{1}H and ^{13}C NMR data are provided in Tables 2 and 3. Compounds **11a**/**b** and **15a**/**b** are new compounds for which the names gerbeloid 5a/gerbeloid 5b and gerbeloid 7a/gerbeloid 7b, respectively, are proposed.

Analysis of the 1D and 2D NMR data of **10** shows the 5-methylcoumarin skeleton (δ 6.99, H-6, δ 7.29, H-7, δ 7.03, H-8 and δ 2.76, CH_3-18) as seen in **14** and **17**, but with an additional double bond (δ 150.0, C-15 and δ 110.6, C-16) and olefinic methylene group (δ 4.52 and 4.46, H-16) appearing and one methyl group disappearing (Tables 1 and 2). Thus, **10** was identified as 4-hydroxy-5-methyl-3-(3-methyl-6-(prop-1-en-2-yl)cyclohex-2-en-1-yl)-2*H*-chromen-2-one, the 10,11-dehydroanalog of an intramolecular domino Knoevenagel ene adduct previously reported [37]. Key COSY and HMBC correlations used for structure elucidation are shown in Figure 4, and **10** is tentatively assigned the 9*S**, 14*R** configuration based on the coupling constants between H-9 and H-14 ($^{3}J_{H9,H14}$ = 10.5 Hz *trans*) as also reported for the synthetic analog [38]. However, keto-enol tautomerism did neither allow chiral separation or acquisition of ECD spectra, and **10** was gradually degraded in solution. ^{1}H NMR, COSY, ROESY, HSQC and HMBC spectra are provided in Figures S56–S60, Supplementary Material, and fully assigned ^{1}H and ^{13}C NMR data are provided in Tables 1 and 2. Compound **10** is a new compound for which the name gerbeloid 4 is proposed.

HRESIMS data for the material eluted with peaks *18-19* and *24-25* provided $[M + H]^+$ ions, showing that these compounds all have the formula $C_{30}H_{28}O_6$ (see details in the Materials and Methods section), suggesting them to be dimers of prenyl-substituted coumarin derivatives. Furthermore, chemical shift values of C-4 (δ 181.7 and 181.9) (Table 4) in **19** and **25**, respectively, showed each of these to consist of a coumarin (lactone) unit and a chromen-4-one (keto) unit, whereas **18** and **25** consist of two coumarin units each. Detailed analyses of 1D and 2D NMR data for **18** and **25** show that they consist of two pyrano[3,2-*c*]coumarin units joined together by bonds between C-9 and C-13′ and between C-10 and C-9′, and comparison with NMR data reported for dibothrioclinin I and II [11], show that **18** and **25** are diastereomers of these. This was further supported by COSY and HMBC correlations (key correlations seen in Figure 7).

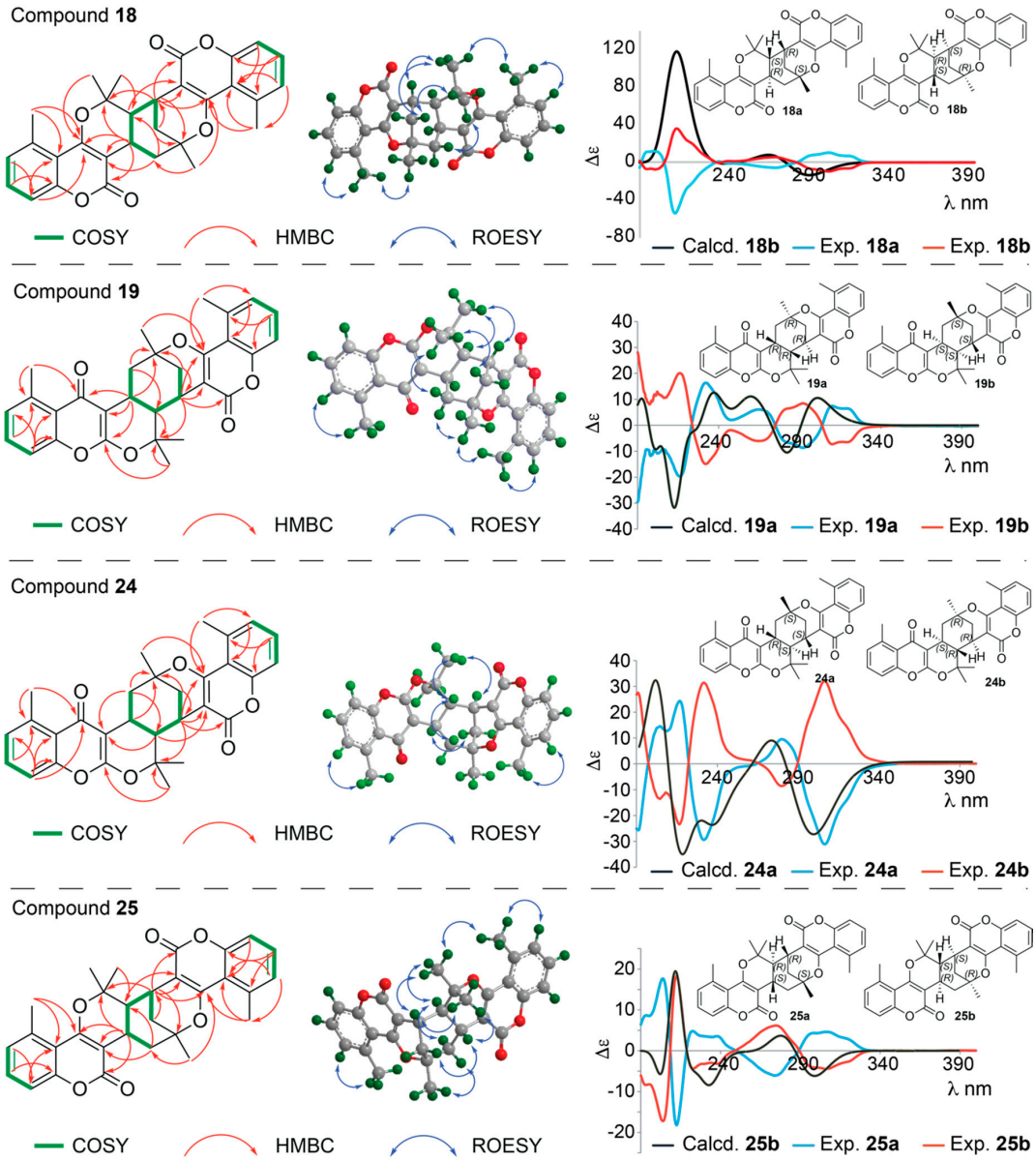

Figure 7. Left: Key COSY and HMBC correlations of **18**, **19**, **24** and **25**. **Middle**: Key ROESY correlations used to establish relative configuration of **18**, **19**, **24** and **25**. **Right**: Calculated ECD spectra of **18b**, **19a**, **24a** and **25b** and experimental ECD spectra of the enantiomers **18a/b**, **19a/b**, **24a/b** and **25a/b**. The enantiomeric structures of **18**, **19**, **24** and **25** are shown with absolute configuration of the stereocenters determined based on the ECD data.

Table 4. ^{13}C NMR (150 MHz) Spectroscopic Data of **18**, **19**, **24**, and **25** [a.]

Pos.	δ_C				Pos.	δ_C			
	18	**19**	**24**	**25**		**18**	**19**	**24**	**25**
2	163.5	163.3	163.9	163.0	2′	165.0	163.8	163.5	163.4
3	103.0	99.6	99.2	102.6	3′	101.3	104.9	109.0	109.0
4	167.5	181.7	181.9	164.2	4′	164.0	166.3	163.1	163.0
4a	115.1	121.5	122.2	115.8	4a′	115.7	115.4	116.0	115.6
5	138.3	141.2	141.3	138.3	5′	138.0	138.3	138.3	138.3
6	128.7	128.7	128.6	128-7	6′	128.5	128.5	128.4	128.8
7	132.4	133.0	131.9	132.1	7′	131.9	132.0	132.7	132.2
8	115.6	116.4	115.4	115.6	8′	115.3	115.9	115.9	115.8
8a	154.9	155.8	155.7	155.1	8a′	154.7	155.1	155.1	155.2
9	28.8	26.2	25.9	26.4	9′	28.9	28.8	26.5	26.7
10	52.9	45.0	54.1	53.1	10′	38.2	31.9	30.2	30.5
11	81.4	86.3	86.4	85.0	11′	83.3	80.8	81.0	81.5
12	23.5	22.4	22.3	23.9	12′	23.6	23.6	23.4	23.7
13	26.8	24.9	28.3	28.9	13′	43.2	40.3	40.1	40.8
14	19.7	28.9	20.5	21.2	14′	27.8	28.3	28.9	29.3

[a] NMR data obtained with samples in methanol-d_4.

The core cyclohexane of **18** was identified as a chair conformation with axial-axial couplings between H-9 and H-10 and between H-9 and H-13′$_{ax}$ ($J_{H9,H10} = J_{H9,H\text{-}13'ax}$ = 12 Hz) and 1,3-diaxial ROEs between H-10, H-10′$_{ax}$, and H-13′$_{ax}$. With equatorial position of H-9′ and CH_3-14′, as seen from coupling constants and ROEs to H-10, H-10′$_{ax}$, and H-13′$_{ax}$, the relative configuration of **18** was established as 9*R**,10*S**,9′*R**,11′*S**. Contrary to this, the core cyclohexane of **25** was identified as a boat conformation, with very strong ROE correlation between H-9 and H-10′$_{endo}$ (and ROEs to H-9′, H-9′, H-13′$_{eq}$ and CH_3-14′ on the same side of the plane) and 1,3-diaxial ROEs between H-10 and H-13′$_{ax}$. The relative configuration of **25** was therefore established as 9*R**,10*S**,9′*S**,11′*R** (Figure 7). Two pairs of enantiomers (**18a** and **18b**, **25a** and **25b**) with the peak area ratios 1:1 were separated by chiral HPLC chromatography (Figures S2 and S3, Supplementary Material). Comparison of the experimental and calculated ECD spectra (Figure 7) allowed assignment of the absolute configurations to be 9*R*,10*S*,9′*R*,11′*S* for **18a** and 9*S*,10*R*,9′*S*,11′*R* for **18b** (with Δ_{ESI} of 0.93), and 9*R*,10*S*,9′*R*,11′*S* for **25a** and 9*S*,10*R*,9′*S*,11′*R* for **25b** (with Δ_{ESI} of 0.82). ^{1}H NMR, COSY, ROESY, HSQC and HMBC spectra are provided in Figures S94–S99 and S118–S123, Supplementary Material, and fully assigned ^{1}H and ^{13}C NMR data are provided in Tables 4 and 5. Compounds **18a**/**b** and **25a**/**b** are new compounds for which the names gerbeloid 9a/gerbeloid 9b and gerbeloid 13a/gerbeloid 13b, respectively, are proposed.

Table 5. ^{1}H NMR (600 MHz) Spectroscopic Data of **18**, **19**, **24**, and **25** [a].

Pos.	δ_H (*J*, in Hz)			
	18	**19**	**24**	**25**
6	7.16, d (7.4 Hz)	7.13, d (7.3 Hz)	7.13, d (7.5 Hz)	7.07, d (7.5 Hz)
7	7.46, dd (8.2, 7.4 Hz)	7.48, dd (8.2, 7.3 Hz)	7.40, dd (8.2, 7.5 Hz)	7.38, dd (8.0, 7.5 Hz)
8	7.19, d (8.2 Hz)	7.24, d (8.0 Hz)	7.15, d (8.2 Hz)	7.11, d (8.0 Hz)
9	2.68, td (12.0, 4.2 Hz)	3.10, br dt (13.1, 6.3 Hz)	2.72, td (12.7, 4.2 Hz)	2.68, td (12.6, 4.2 Hz)
10	2.17, dd (12.0, 1.9 Hz)	2.15, br d (6.6 Hz)	1.62, dd (12.4, 3.2 Hz)	1.62, dd (12.4, 3.1 Hz)
12	2.70, s	2.76, s	2.78, s	2.69, s
13	1.91, s	1.67, s	1.79, s	1.87, s
14	1.10, s	1.77, s	1.43, s	1.44, s
6′	7.09, d (7.4 Hz)	7.15, d (7.5 Hz)	7.09, d (7.6 Hz)	7.10, d (7.8 Hz)
7′	7.39, dd (8.4, 7.4 Hz)	7.44, dd (8.3, 7.5 Hz)	7.46, dd (8.4, 7.6 Hz)	7.41, dd (8.3, 7.8 Hz)
8′	7.12, d (8.4 Hz)	7.17, d (8.3 Hz)	7.21, d (8.4 Hz)	7.15, d (8.3 Hz)
9′	3.59, q (2.7 Hz)	3.50, br q	3.08, q (3.2 Hz)	3.13, q (3.1 Hz)
10′	2.22, dd (13.2, 2.8 Hz) 1.90, dt (13.2, 2.8 Hz)	2.31, dd (14.1, 2.8 Hz); 1.82, dt (14.1, 2.5 Hz)	2.29, dd (14.0, 3.4 Hz); 1.53, dd (14.0, 2.6 Hz)	2.28, dd (13.9, 3.4 Hz); 1.55, dd (13.9, 2.7 Hz)
12′	2.81, s	2.84, s	2.73, s	2.74, s
13′	3.51, ddd (14.0, 4.2, 2.6 Hz); 1.47, dd (14.0, 12.0 Hz)	3.02, ddd (14.2, 5.5, 2.5 Hz); 1.71, dd (14.2, 13.1 Hz)	3.80, dd (14.7, 4.2 Hz); 1.40 dd (14.7, 13.1 Hz)	3.68, dd (14.8, 4.3 Hz); 1.48, dd (14.8, 13.0 Hz)
14′	1.61, s	1.61, s	1.78, s	1.76, s

[a] NMR data obtained with samples in methanol-d_4.

The ^{1}H NMR data of **19** and **24** show similar patterns for H-6, H-7, H-8 and H-6′, H-7′, H-8′ in the aromatic region as seen for **18** and **25**, showing the methyl groups at C-5 and C-5′. However, as stated above, **19** and **24** each consist of a coumarin (seen from the chemical shift values of δ 163.8 and δ 163.5 for C-2′ and δ 166.3 and δ 163.1 for C-4′ in **19** and **24**, respectively) and a chromen-4-one unit (seen from the chemical shift values of δ 163.3 and δ 163.9 for C-2 and δ 181.7 and δ 181.9 for C-4 in **19** and **24**, respectively). HMBC correlations from CH_3-18 and H-9 to C-2, from H-9 and H-10 to C-3, and from H-8 and CH_3-12 to C-4 support the pyrano[2,3-*b*]chromen-4-one skeleton, whereas HMBC correlations from H-9′ to C-2′, H-9′ and H-10 to C-3′, and from CH_3-14′ to C-4′ support the pyrano[3,2-*c*]coumarin skeleton (Figure 7). Furthermore, HMBC correlations from H-9 to C-11′ and C-13′ as well as from H-10 to C-3′ and C-9′ and from H-9′ to C-10 and C-11 proved the bridging between the pyrano[2,3-*b*]chromen-4-one and the pyrano[3,2-*c*]coumarin skeleton as shown in Figures 3 and 7. Based on analysis of coupling constants and ROESY correlations (Figure 7), **19** was assigned the relative configuration 9*R**,10*R**,9′*R**,11′*R** and **24** was assigned the relative configuration 9*R**,10*S**,9′*S**,11′*S**. Additionally, X-ray crystal structure analysis of the racemate of **19** yielded the structure shown in perspective drawing (ORTEP-3) [39] in Figure 8. This agrees with the structure established based on the NMR data, confirming the 9*R**,10*R**,9′*R**,11′*R** configuration of **19**.

After chiral separation of **19** and **24** (1:1 ratios of enantiomers **19a**, **19b** and **24a**, **24b**, see Figures S2 and S3, Supplementary Material), ECD spectra of both pairs of enantiomers were acquired. These are shown in Figure 7, and comparison with the calculated ECD spectra of **19a** and **24a** allowed assignment of the absolute configurations to be 9*R*,10*R*,9′*R*,11′*R* for **19a** and 9*S*,10*S*,9′*S*,11′*S* for **19b** (with Δ_{ESI} of 0.77), and 9*R*,10*S*,9′*S*,11′*S* for **24a** and 9*S*,10*R*,9′*R*,1′*R* for **24b** (with Δ_{ESI} of 0.87) (Figure 7). ^{1}H NMR, COSY, ROESY, HSQC and HMBC spectra are provided in Figures S100–S105 and S112–S117, Supplementary Material, and fully assigned ^{1}H and ^{13}C NMR data are provided in Tables 4 and 5. Compounds **19a**/**b** and **24a**/**b** are new compounds for which the names gerbeloid 10a/gerbeloid 10b and gerbeloid 12a/gerbeloid 12b, respectively, are proposed.

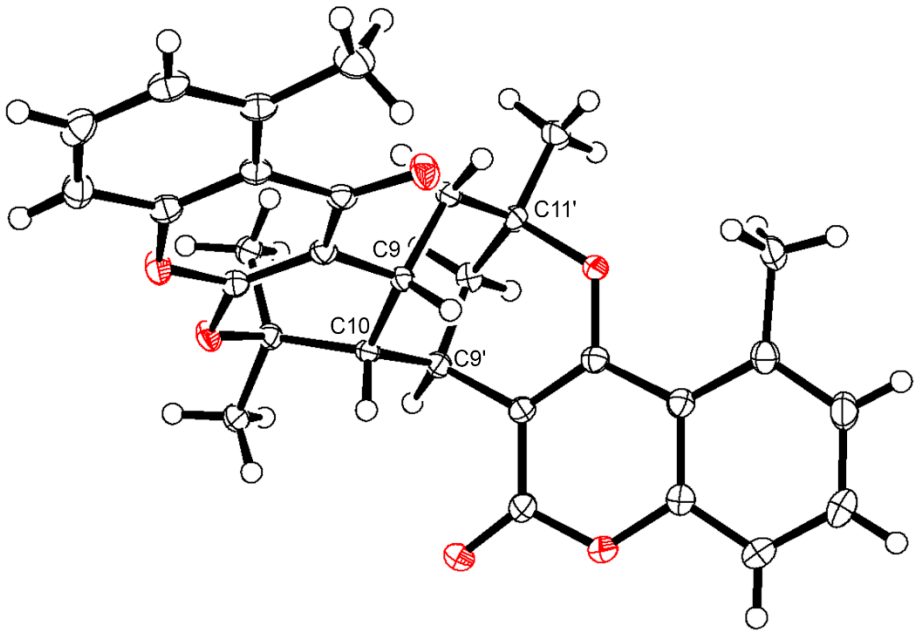

Figure 8. Perspective drawing (ORTEP-3) of **19**. Displacement ellipsoids of the non-hydrogen atoms are shown at the 50% probability level. Hydrogen atoms have been shown as spheres of arbitrary size. Oxygen atoms are red.

Compound **23** showed a $[M + H]^+$ ion with *m/z* 311.1641 ($C_{20}H_{23}O_3^+$, ΔM 0.2 ppm) and a $[M + Na]^+$ ion with *m/z* 333.1446 ($C_{20}H_{22}O_3Na^+$, ΔM 4.5 ppm), which suggested the molecular formula $C_{20}H_{22}O_3$, with a hydrogen deficiency index of 10. The ^1H and ^{13}C NMR spectra of **23** show signals corresponding to H-6, H-7 and H-8 in the aromatic region and the methyl group at C-5 as well as characteristic chemical shifts for C-2 (δ 165.2), C-3 (δ 103.9), and C-4 (δ 163.6) as also observed for **14** and **17**, suggesting they share the same 5-methylcoumarin skeleton. The pyrano[3,2-*c*]coumarin core skeleton is supported by HMBC correlations from CH_3-16 and CH_3-17 to C-4, from CH_3-17 to C-10, and from H-9 to C-2 and C-4 (Figure 9) as well as correlations in the COSY spectrum between H-9 and H-10. In fact, the COSY spectrum showed correlations corresponding to the H-9 ↔ H-10 ↔ H-14 ↔ H-13 ↔ H-12 spin system, and HMBC correlations from H-12 to C-11 and C-17 revealed the cyclopentane ring system, whereas HMBC correlations from H-9, H-14, CH_3-18 and CH_3-19 to C-15 and from H-18 and H-19 to C-9 and C-14 revealed the dimethylated cyclobutane ring system. Thus, **23** was identified as a 5-methylcoumarin with a 6/5/4 ring system fused at C-3 and C-4. Two coumarins with similar 6/5/4 ring systems have been reported before [40], but linked to either C-5 and C-6 or C-7 and C-8 of the coumarin moiety; and the NMR data for the 6/5/4 ring system of the previously reported compounds resemble those observed for **23** (Tables 2 and 3) [40,41]. The coupling constants between H-9 and H-10 (^3J = 9.4 Hz) and between H-10 and H-14 (^3J = 8.1 Hz) are in close agreement with those previously reported for a similar 6/5/4 ring system with H-9, H-10 and H-14 being *cis*, and thus on the same side of the molecule. Similarly, the ROESY correlations between H-9 ↔ H-18 ↔ H-14 ↔ H-13A and H-10 ↔ H-17 ↔ H-12A show these to be on one plane of the molecule, whereas ROESY correlations between H-19 and H12B/H-13B shows these to be on the other plane of the molecule - and thus the relative configuration of **23** is 9*R**,10*R**,11*R**,14*S**.

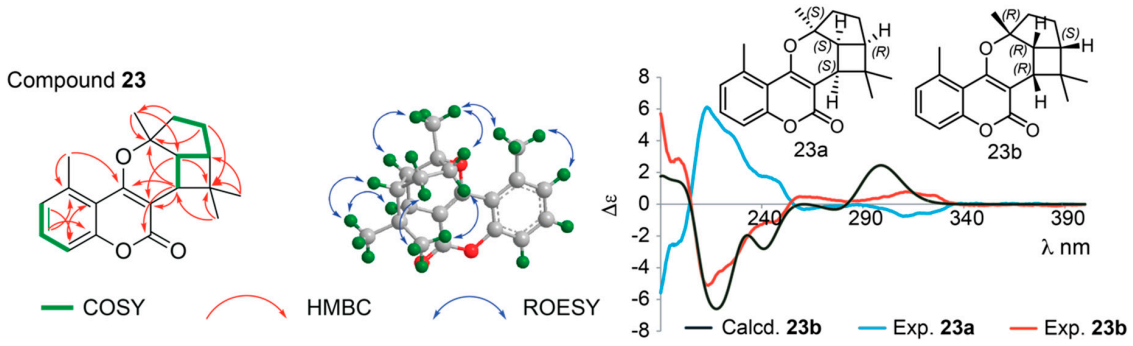

Figure 9. Left: Key COSY and HMBC correlations of **23**. **Middle**: Key ROESY correlations to establish relative configuration of one of the enantiomers of **23**. **Right**: Calculated ECD spectra of **23b** and experimental ECD spectra of the enantiomers **23a/b**. The enantiomeric structures of **23** shown with absolute configuration of the stereocenters determined based on the ECD data.

Chiral resolution of **23** gave two enantiomers (**23a** and **23b**) in a 1:1 ratio (Figure S2, Supplementary Material), and comparison of the ECD spectra of **23a** and **23b** with the ECD spectrum calculated for **23b** (Figure 9), allowed assignment of the absolute configuration to be 9*R*,10*R*,11*R*,14*S* for **23a** and 9*S*,10*S*,11*S*,14*R* for **23b**, respectively, with Δ_{ESI} of 0.88. ^{1}H NMR, COSY, ROESY, HSQC and HMBC spectra are provided in Figures S106–S111, Supplementary Material, and fully assigned ^{1}H and ^{13}C NMR data are provided in Tables 2 and 3. Compounds **23a**/**b** are new compounds for which the names gerbeloid 11a/gerbeloid 11b are proposed.

The material eluted with peaks *14–19* and *23–25* were correlated with both α-glucosidase and PTP1B inhibitory activity in the high-resolution inhibition profile (Figures 1 and 2). Due to limited amount of material isolated of the racemic mixtures as well as the individual enantiomers after chiral separation, it was not possible to make dilution series to obtain full dose-response curves. However, for the racemic mixtures of **17**–**19**, **24** and **25**, it was possible to test the inhibitory activity at a single concentration between 32.2 and 201.6 μM. The results are provided in Table 6 and show that the tested compounds show weak to moderate inhibitory activity towards both α-glucosidase and PTP1B.

Table 6. Percentage inhibition of **17**–**19**, **24** and **25** against α-glucosidase and PTP1B at the concentration shown in brackets.

Compound	α-Glucosidase (μM)	PTP1B (μM)
17	32% (201.6)	N.D.[a]
18	40% (159.1)	N.D.[a]
19	48% (129.1)	67% (64.4)
24	51% (129.1)	47% (32.2)
25	45% (64.4)	32% (129.1)

[a] N.D. Not detected.

The reported values may be underestimated, because typically only one enantiomer of a racemic mixture is an active inhibitor of the target enzyme. Thus, isolation of more material and subsequent chiral separation are needed to obtain full dose-response curves for both enantiomers in both the α-glucosidase and the PTP1B assay, as well as for being able to study the mode of inhibition of the many compounds correlated with one or both activities. The only prior study with dual inhibitory activity of PTP1B and α-glucosidase with this kind of compounds, is a recent study with a series of prenylated coumarins from *Angelica decursiva*, showing weak α-glucosidase inhibitory activity with IC_{50} values ranging from 65 to 172 μM, and PTP1B inhibitory activity with IC_{50} values ranging from 5 to 59 μM.

The coumarin skeleton is synthesized from acetyl-CoA and malonyl-CoA through the polyketide pathway in plants [42]. Inspired by the biosynthetic pathway of tetrahydrocannabinolic acid (THCA)

in *Cannabis sativa* [43], the monoterpenoid-coumarins identified in this study are plausibly first added a monoterpenoid chain to C-3 of the coumarin skeleton, catalyzed by prenyl transferase (Pathway 1 in Figure 10). As mentioned above, [4 + 2] cycloaddition reactions have been utilized for the total synthesis of structures similar to **11**, **14**, **15** and **17** (Scheme S1, Supplementary Material) [38], and therefore cyclisations via different Diels-Alder cycloadditions between the monoterpenoid and coumarin, followed by oxidations or reductions catalyzed by oxidoreductase enzymes, could be involved in the formation of **2**, **6**, **7**, **10**, **11**, **14**–**17** and **23** (Figure 10).

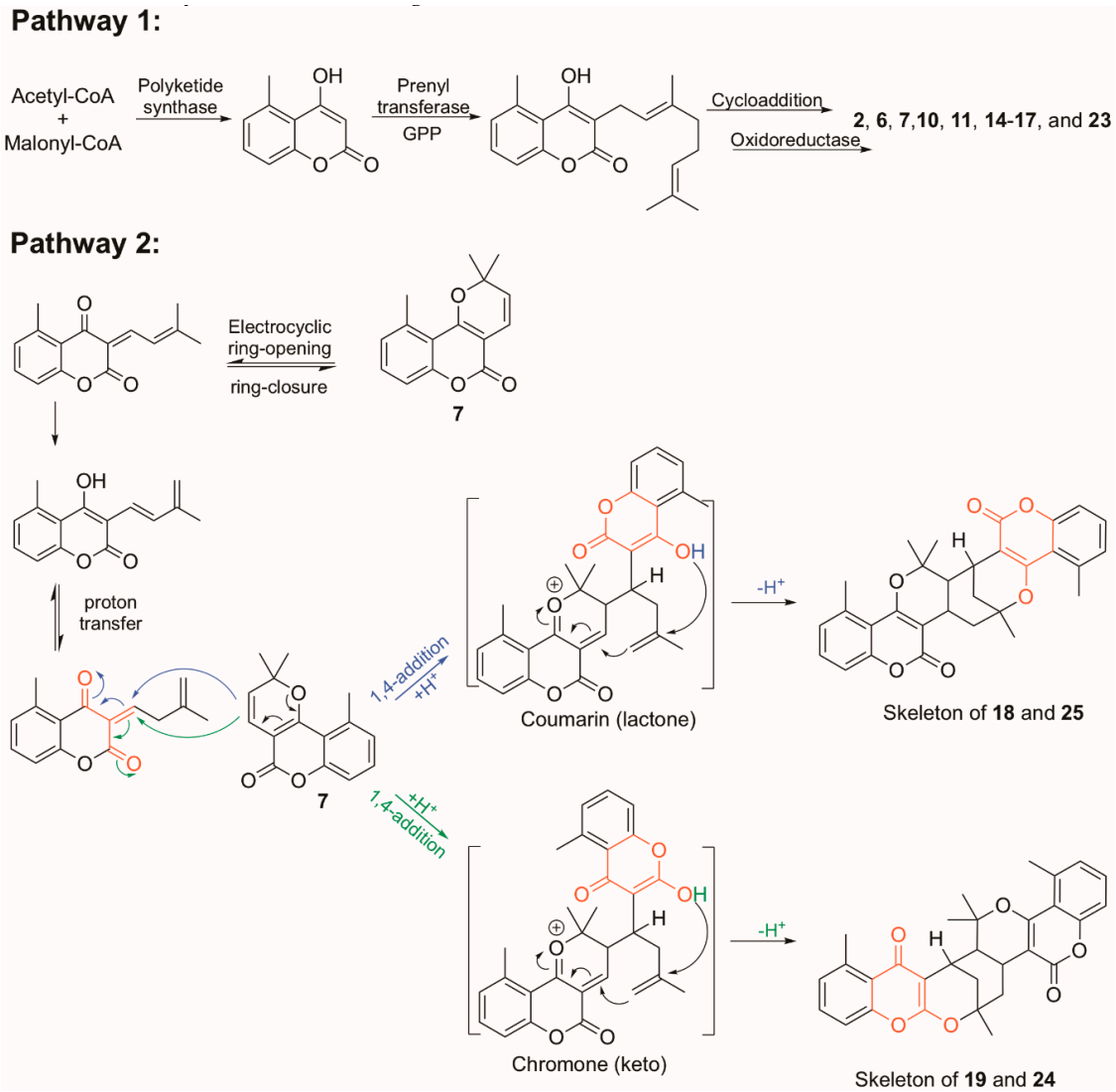

Figure 10. Possible biosynthetic pathway for the prenyl- and geranyl substituted coumarin derivatives isolated in this study.

There are no prior studies on the biosynthesis of coumarins related to the dimeric coumarin derivatives isolated in this study, but total synthesis of pyranylquinoline alkaloids [44] suggests mechanisms for the plausible biosynthetic route for **18**, **19**, **24** and **25** presented as pathway 2 in Figure 10. In this route, the precursor of **18**, **19**, **24** and **25** is suggested to be **7**, which is seen as a major peak in the ethyl acetate extract of *G. piloselloides* (Figure 1). The key steps in the dimerization of **7** include a ring opening, a hydride shift and a 1,4-addition (Figure 10), followed by 1,4-addition reactions leading to **18** and **25** with two coumarin moieties or **19** and **24** with one coumarin moiety and one chromone moiety in the structure (Figure 10).

3. Materials and Methods

3.1. Plant Material and Extraction Procedure

Aerial parts of *Gerbera piloselloides* (L.) Cass was collected from Sandaohe Village, Duyun City, Guizhou Province, People's Republic of China in September 2017 and authenticated by Associate Prof. Chunhua Liu (Provincial Key Laboratory of Pharmaceutics in Guizhou Province, Guizhou Medical University). A voucher specimen (accession number JX20170208) is deposited at the Guizhou Medical University. The air-dried material (1.7 kg) was milled and extracted three times with 2 L ethyl acetate (1 h of ultra-sonication for each extraction). The combined extracts were filtered and concentrated under reduced pressure to give 20 g of dark green crude extract.

3.2. Chemicals and Reagents

Recombinant human protein tyrosine phosphatase 1B (PTP1B) (BML-SE332-0050, EC 3.1.3.48) was purchased from Enzo Life Sciences (Farmingdale, NY, USA). α-Glucosidase from *Saccharomyces cerevisiae* type I, lyophilized powder (EC 3.2.1.20), *p*-nitrophenyl α-D-glucopyranoside (*p*-NPG), *p*-nitrophenyl phosphate (*p*NPP), acarbose, sodium phosphate monobasic dihydrate, disodium phosphate dibasic, sodium azide, sodium chloride, dimethyl sulfoxide (DMSO), tris-(hydroxymethyl)-aminomethane (Tris), bis-(2-hydroxyethyl)-imino-tris-(hydroxymethylmethane) (Bis-Tris), *N*,*N*,*N*′,*N*′-ethylenediaminetetraacetate (EDTA), dithiothreitol (DTT), methanol-d_4, and HPLC grade acetonitrile were purchased from Sigma-Aldrich (St. Louis, MO, USA), and formic acid (FA) was purchased from Merck (Darmstadt, Germany). Water was purified by deionization and filtration through a 0.22 μm membrane (Millipore, Billerica, MA, USA).

3.3. LC-PDA-HRMS

LC-PDA-HRMS analyses were performed on a model 1260 analytical-scale HPLC system consisting of a G1322A degasser, a G1311A quaternary pump, a G1316A thermostatted column compartment, and a G1315A photodiode-array detector (Agilent, Santa Clara, CA, USA) and a Bruker micrOTOF-Q II high-resolution mass spectrometer (Bruker Daltonik, Bremen, Germany). The column eluate was connected to a T-piece splitter directing 1% of the flow to the mass spectrometer and 99% of the flow the photodiode-array detector. The micrOTOF-Q II mass spectrometer, equipped with an ESI source, was operated in the positive-ion mode using a drying temperature of 200 °C, a capillary voltage of 4100 V, a nebulizer pressure of 2.0 bar, and a drying gas flow of 7 L/min. A solution of sodium formate clusters was injected automatically at the beginning of each run to enable internal mass calibration. Chromatographic separations were performed at 40 °C on a Luna C_{18}(2) column, 150 × 4.6 mm i.d., 3 μm particle size, 100 Å pore size (Phenomenex, Torrance, CA, USA) at a flow rate of 0.5 mL/min and using a binary gradient of mobile phase A (CH_3CN:H_2O 5:95 + 0.1% FA) and mobile phase B (CH_3CN:H_2O 95:5 + 0.1% FA). Chromatographic separation and mass spectrometry were controlled using Hystar ver. 3.2 software (Bruker Daltonik).

3.4. Dual High-Resolution PTP1B/α-Glucosidase Inhibition Profiling

High-performance liquid chromatography (HPLC) was performed with an Agilent 1200 series instrument consisting of a G1322A degasser, a G1311A quaternary solvent pump, a G1313A high-performance auto sampler, a G1316A thermostatic column compartment, a G1315B photodiode-array detector, and a G1364C fraction collector, all controlled by Agilent ChemStation software ver. B.03.02. 10 μL of crude extract (50 mg/mL in methanol) was separated at 40 °C on a Phenomenex Luna C_{18}(2) column (150 mm × 4.6 mm i.d., 3 μm particle size, 100 Å pore size), using the following binary elution gradient of mobile phase A (CH_3CN:H_2O 5:95 + 0.1% FA) and mobile phase B (CH_3CN:H_2O 95:5 + 0.1% FA) at a flow rate of 0.5 mL/min: 0 min, 10% B; 30 min, 80% B; 50 min, 100% B and 65 min, 100% B. The eluate from 2 to 65 min was fractionated into 176 wells of two 96-well plates (excluding 8 wells in each plate for the blank control), to give a resolution of 2.8 data points

per min. 10 μL of fraction F2 was separated at 40 °C on a Kinetex pentafluorophenyl (PFP) column (150 mm × 4.6 mm i.d., 2.6 μm particle size, 100 Å pore size) (Phenomenex) using the following binary elution gradient of mobile phase C (MeOH:H_2O 5:95 + 0.1% FA) and mobile phase D (MeOH:H_2O 95:5 + 0.1% FA) at a flow rate of 0.5 mL/min: 0 min, 60% D; 15 min, 80% D; 30 min, 100% D and 45 min, 100% D. The eluate from 2 to 40 min was fractionated into one 96-well plate (88 wells) to give a resolution of 2.3 data points per min. The fractions in all wells were subsequently evaporated to dryness under reduced pressure, and after PTP1B and a-glucosidase assaying, dual high-resolution PTP1B/α-glucosidase inhibition profiles of crude extract and fraction F2 were constructed as detailed by Wubshet and coworkers [45].

3.5. Targeted Isolation of PTP1B/α-Glucosidase Inhibitors and Major Metabolites

Crude ethyl acetate extract (100 mg/mL in MeOH) was separated using a preparative-scale Agilent 1100 HPLC system comprising two G1361A preparative-scale solvent delivery pumps, a G2260A autosampler, and a G1365B multiple wavelength detector, controlled by Agilent ChemStation software ver. B.01.01. Injections (900 μL) were separated at room temperature on a Phenomenex Luna C_{18} column (250 mm × 21.2 mm i.d., 5 μm particle size) using the following binary gradient of mobile phase A and B, *vide supra*, at a flow rate of 17 mL/min: 0 min, 10% B; 30 min, 80% B; 50 min, 100% B, 65 min, 100% B. Manual collection of eluate from 15.8 to 16.5 min (peak *1*), 17.8 to 18.6 min (peak *2*), 25.0 to 25.6 min (peak *3*), 25.8 to 26.2 min (peak *4*), 26.3 to 26.7 min (peak *5*), 26.8 to 28.1 min (peak *6*), 30.1 to 31.3 min (peak *7*), 32.0 to 32.5 min (peak *8*), 32.5 to 33.1 min (peak *9*), 35.7 to 39.6 min (Fraction 1), 39.8 to 41.5 min (Fraction 2), 41.6 to 42.3 min (peak *23*), 42.7 to 43.4 min (peak *24*), 44.2 to 44.9 min (peak *25*) and 53.1 to 54.4 min (peaks *26-27*) afforded 11 mg of peak *1*, 10 mg of peak *2*, 14.2 mg of peak *3*, 9.4 mg of peak *5*, 10.8 mg of peak *6*, 85.6 mg of peak *7*, 9.8 mg of peak *8*, 51.1 mg of peak *9*, 54.2 mg of Fraction 1, 67.0 mg of Fraction 2, 13.1 mg of peak *23*, 7.8 mg of peak *24*, 12.8 mg of peak *25* and 4.4 mg of peaks *26–27*. Compounds **5** and **6** were purified from the material eluted as peaks *5* and *6* on the above-mentioned analytical-scale HPLC system and PFP column (10 μL injections of a 25 mg/mL solution, flow rate 0.5 mL/min) using the following binary gradient elution profile of mobile phase C and D: 0 min, 60% D; 15 min, 80% D; 35 min, 90% D; 45 min, 100% D and 47 min, 60% D. This yielded 1.2 mg of **5** (t_R = 10.6 min) and 1.0 mg of **6** (t_R = 14.3 min). Compounds **10-12** were purified from fraction F1 (10 μL injections of a 20 mg/mL solution, flow rate 0.5 mL/min) using the following binary gradient elution profile of mobile phase C and D: 0 min, 70% D; 10 min, 80% D; 30 min, 81% D; 45 min, 90% D and 55 min, 100% D. This afford 0.7 mg of **10** (t_R = 17.0 min), 1.2 mg of **11** (t_R = 18.6 min) and 0.8 mg of **12** (t_R = 19.5 min). Compounds **14–19** were purified from fraction F2 (10 mL injections of a 20 mg/mL solution, flow rate 0.5 mL/min) using the following binary gradient elution profile of mobile phase C and D: 0 min, 60% D; 15 min, 80% D; 30 min, 100% D, 45 min, 100% D. This yielded 1.6 mg of **14** (t_R = 26.3 min), 1.5 mg of **15** (t_R = 27.0 min), 2.5 mg of **16** (t_R = 28.2 min), 2.1 mg of **17** (t_R = 29.1 min), 1.2 mg of **18** (t_R = 31.5 min), and 1.7 mg of **19** (t_R = 31.8 min). Compounds **23**, **24** and **25** were purified after repeated separation of the material eluted as peaks *23*, *24* and *25* (15 mL injections of a 25 mg/mL solution) using the following binary gradient of mobile phase C and D as indicated after each compound: **23** (t_R = 28.4 min): 0 min, 60% D; 15 min, 80% D; 30 min, 100% D; 45 min, 100% D and 47 min, 60% D; **24** (t_R = 26.0 min) and **25** (t_R = 27.0 min): 0 min, 70% D; 10 min, 90% D; 35 min, 95% D; 45 min, 100% D and 55 min, 100% D. This gave 1.5 mg of **23**, 1.1 mg of **24** and 1.7 mg of **25**.

3.6. Chiral Separation of Enantiomers

Chiral resolution of **6**, **15**, **18**, **19**, **23**, **24** and **25** was performed at room temperature on a Dionex Ultimate instrument consisting of a LPG-3200BX pump and a MWD-3000SD UV detector, both controlled by Chromeleon software ver. 6.80 (Thermo Fisher Scientific, Waltham, Ca, USA), and with a Rheodyne 9725I injector with 10 μL loop. Enantiomers of compounds **6**, **15**, **18**, **19**, **23** and **24** were separated at a flow rate of 1 mL/min on a Chiralpak AD-H column (250 × 4.6 mm i.d., 5.0 μm particle size) (Chiral Technologies, West Chester, PA, USA) isocratically eluted with the following mixtures

of isopropanol (mobile phase E) and heptane (mobile phase F): 20% E and 80% F for **6**; 1% E and 99% F for **15**; 10% E and 90% F for **18**, **19** and **24**; 5% E and 95% F for **23** and **24**. Enantiomers of compound **14** were separated at a flow rate of 0.8 mL/min on a Chiralpak OD-H column (250 × 4.6 mm i.d., 5.0 µm particle size) (Chiral Technologies) isocratically eluted at room temperature with 2% E and 98% F. Enantiomers of compounds **11** and **17** were separated at a flow rate of 1 mL/min on a Lux Amylose-2 column (250 × 4.6 mm i.d., 5.0 µm particle size) (Chiral Technologies) isocratically eluted with 1% E and 99% F. The chiral resolution of ten pairs of enantiomers gave 0.40 mg/0.40 mg of **6a/b**, 0.15 mg/0.15 mg of **11a/b**, 0.20 mg/0.20 mg of **14a/b**, 0.20 mg/0.17 mg of **15a/b**, 0.50 mg/0.40 mg of **17a/b**, 0.17 mg/0.20 mg of **18a/b**, 0.20 mg/0.20 mg of **19a/b**, 0.19 mg/0.15 mg of **23a/b**, 0.30 mg/0.20 mg of **24a/b** and 0.18 mg/0.20 mg of **25a/b**.

Compound **2**: white, amorphous powder; insufficient material available for optical rotation; HPLC-UV (MeOH in H_2O + 0.1% FA) λ_{max} 203, 230, 282-293 nm; ^1H and ^{13}C NMR data, see Tables 1 and 3; ECD (*c* 9.0 mM, CH_3CN) λ_{max} ($\Delta\varepsilon$) 207 (−7.1), 223.5 (+1.02), 264 (+0.31), 294 (+0.91) nm; (+)HRESIMS *m/z* $[M + H]^+$ calcd for $C_{15}H_{17}O_5{}^+$, 277.1071, found 277.1083, ΔM −4.5 ppm.

Compound **5**: white, amorphous powder; insufficient material available for optical rotation; HPLC-UV (MeOH in H_2O + 0.1% FA) λ_{max} 199, 260, 294 nm; ^1H and ^{13}C NMR data, see Tables 1 and 3; (+)HRESIMS *m/z* $[M + H]^+$ calcd for $C_{18}H_{23}O_3{}^+$, 287.1642, found 287.1637, ΔM +1.6 ppm; $[M + Na]^+$ calcd for $C_{18}H_{22}O_3Na^+$, 309.1461, found 309.1463, ΔM −0.6 ppm.

Compound **6**: white, amorphous powder; insufficient material available for optical rotation; HPLC-UV (MeOH in H_2O + 0.1% FA) λ_{max} 198, 212, 248, 348 nm; ^1H and ^{13}C NMR data, see Tables 1 and 3; (+)HRESIMS *m/z* $[M + H]^+$ calcd for $C_{20}H_{23}O_5{}^+$, 343.1540, found 343.1527, ΔM +3.8 ppm; $[M + Na]^+$ calcd for $C_{20}H_{22}O_5Na^+$, 365.1359, found 365.1355, ΔM +1.2 ppm.

Compound **6a:** ECD (*c* 5.8 mM, CH_3CN) λ_{max} ($\Delta\varepsilon$) 201 (−19.0), 220 (+14.0), 250 (+7.1), 282 (−2.2), 312 (+4.4), 325 (+3.6) nm.

Compound **6b:** ECD (*c* 5.8 mM, CH_3CN) λ_{max} ($\Delta\varepsilon$) 201 (+19.0), 220 (−14.0), 250 (−7.1), 282 (+2.2), 312 (−4.4), 325 (−3.6) nm.

Compound **8**: white, amorphous powder; $[\alpha]_D{}^{25}$ + 60.8 (*c* 7.2 mM MeOH); HPLC-UV (MeOH in H_2O + 0.1% FA) λ_{max} 204, 235, 266, 365 nm; ^1H NMR data, see Table S1, Supplementary Material; ECD (*c* 6.3 mM, CH_3CN) λ_{max} ($\Delta\varepsilon$) 195 (+17.5), 223.5 (−8.2), 266.1 (+2.3) nm; (+)HRESIMS *m/z* $[M + H]^+$ calcd for $C_{18}H_{23}O_5{}^+$, 319.1540, found 319.1535, ΔM +1.6 ppm.

Compound **10**: white, amorphous powder; insufficient material available for optical rotation; HPLC-UV (MeOH in H_2O + 0.1% FA) λ_{max} 207, 225-237, 294, 310 nm; ^1H and ^{13}C NMR data, see Tables 1 and 3; (+)HRESIMS *m/z* $[M + H]^+$ calcd for $C_{20}H_{23}O_3{}^+$, 311.1642, found 311.1644, ΔM −0.7 ppm; $[M + Na]^+$ calcd for $C_{20}H_{22}O_3Na^+$, 333.1461, found 333.1460, ΔM +0.3 ppm.

Compound **11**: white, amorphous powder; insufficient material available for optical rotation; HPLC-UV (MeOH in H_2O + 0.1% FA) λ_{max} 207, 229, 275, 299 nm; ^1H and ^{13}C NMR data, see Tables 1 and 3; (+)HRESIMS *m/z* $[M + H]^+$ calcd for $C_{20}H_{23}O_3{}^+$, 311.1642, found 311.1644, ΔM −0.7 ppm; $[M + Na]^+$ calcd for $C_{20}H_{22}O_3Na^+$, 333.1461, found 333.1460, ΔM +0.3 ppm.

Compound **11a:** ECD (*c* 2.4 mM, CH_3CN) λ_{max} ($\Delta\varepsilon$) 193 (+4.0), 223 (−2.2), 300 (−0.2) nm.

Compound **11b:** ECD (*c* 2.4 mM, CH_3CN) λ_{max} ($\Delta\varepsilon$) 193 (−6.5), 223 (+3.7), 300 (+0.8) nm.

Compound **12**: white, amorphous powder; insufficient material available for optical rotation; HPLC-UV (MeOH in H_2O + 0.1% FA) λ_{max} 200, 231, 260, 300–310 nm; ^1H NMR data, see Table S1, Supplementary Material; (+)HRESIMS *m/z* $[M + H]^+$ calcd for $C_{18}H_{23}O_2{}^+$, 271.1693, found 271.1701, ΔM −3.1 ppm; $[M + Na]^+$ calcd for $C_{18}H_{22}O_2Na^+$, 293.1512, found 293.1515, ΔM −1.0 ppm.

Compound **14**: white, amorphous powder; insufficient material available for optical rotation; HPLC-UV (MeOH in H_2O + 0.1% FA) λ_{max} 206, 227, 283-306, 319 nm; ^1H and ^{13}C NMR data, see Tables 1

and 3; (+)HRESIMS *m/z* [M + H]$^+$ calcd for $C_{20}H_{23}O_3^+$, 311.1642, found 311.1644, ΔM −0.7 ppm; [M + Na]$^+$ calcd for $C_{20}H_{22}O_3Na^+$, 333.1461, found 333.1460, ΔM +0.3 ppm.

Compound **14a:** ECD (*c* 3.2 mM, CH_3CN) λ_{max} (Δε) 194 (−1.0), 210 (+2.0), 237 (+0.5), 280 (−0.4) nm.

Compound **14b:** ECD (*c* 3.2 mM, CH_3CN) λ_{max} (Δε) 194 (+1.2), 210 (−1.7), 233 (−0.5), 280 (+0.5) nm.

Compound **15**: white, amorphous powder; insufficient material available for optical rotation; HPLC-UV (MeOH in H_2O + 0.1% FA) λ_{max} 206, 231, 278–298 nm; ^{1}H and ^{13}C NMR data, see Tables 2 and 3; (+)HRESIMS *m/z* [M + H]$^+$ calcd for $C_{20}H_{23}O_3^+$, 311.1642, found 311.1644, ΔM −0.7 ppm; [M + Na]$^+$ calcd for $C_{20}H_{22}O_3Na^+$, 333.1461, found 333.1460, ΔM +0.3 ppm.

Compound **15a:** ECD (*c* 3.2 mM, CH_3CN) λ_{max} (Δε) 190 (+19.3), 215 (−10.5), 250 (−1.9), 273 (−3.9), 292 (−3.6) nm.

Compound **15b:** ECD (*c* 2.7 mM, CH_3CN) λ_{max} (Δε) 190 (−21.6), 215 (+13.5), 250 (+3.3), 273 (+5.0), 292 (+4.7) nm.

Compound **17**: white, amorphous powder; insufficient material available for optical rotation; HPLC-UV (MeOH in H_2O + 0.1% FA) λ_{max} 207, 221, 293–309 nm; ^{1}H and ^{13}C NMR data, see Tables 2 and 3; (+)HRESIMS *m/z* [M + H]$^+$ calcd for $C_{20}H_{23}O_3^+$, 311.1642, found 311.1644, ΔM −0.7 ppm; [M + Na]$^+$ calcd for $C_{20}H_{22}O_3Na^+$, 333.1461, found 333.1460, ΔM +0.3 ppm.

Compound **17a:** ECD (*c* 5.9 mM, CH_3CN) λ_{max} (Δε) 194 (−3.1), 211 (+11.1), 279 (−0.7), 308 (+1.1), 323 (+0.9) nm.

Compound **17b:** ECD (*c* 6.4 mM, CH_3CN) λ_{max} (Δε) 194 (+3.5), 211 (−10.9), 280 (+1.2), 309 (−1.3), 325 (−0.7) nm.

Compound **18**: white, amorphous powder; insufficient material available for optical rotation; HPLC-UV (MeOH in H_2O + 0.1% FA) λ_{max} 208, 218, 292–321 nm; ^{1}H and ^{13}C NMR data, see Tables 2 and 3; (+)HRESIMS *m/z* [M + H]$^+$ calcd for $C_{30}H_{29}O_6^+$, 485.1959, found 485.1943, ΔM +3.2 ppm; [M + Na]$^+$ calcd for $C_{30}H_{28}O_6Na^+$, 507.1778, found 507.1760, ΔM +3.6 ppm.

Compound **18a:** ECD (*c* 1.7 mM, CH_3CN) λ_{max} (Δε) 198 (+11.7), 212 (−54.0), 275 (−5.7), 308 (+10.3) nm.

Compound **18b:** ECD (*c* 2.0 mM, CH_3CN) λ_{max} (Δε) 199 (−7.5), 212 (+35.9), 275 (+5.5), 308 (−9.6) nm.

Compound **19**: Colourless needle crystals (CD_3OD); insufficient material available for optical rotation; HPLC-UV (MeOH in H_2O + 0.1% FA) λ_{max} 206, 221, 277–291 nm; ^{1}H and ^{13}C NMR data, see Tables 2 and 3; (+)HRESIMS *m/z* [M + H]$^+$ calcd for $C_{30}H_{29}O_6^+$, 485.1959, found 485.1943, ΔM +3.2 ppm; [M + Na]$^+$ calcd for $C_{30}H_{28}O_6Na^+$, 507.1778, found 507.1760, ΔM +3.6 ppm.

Compound **19a:** ECD (*c* 2.0 mM, CH_3CN) λ_{max} (Δε) 190 (−29.5), 202 (−10.7), 216 (−19.7), 233 (+16.3), 249 (+2.1), 266 (+6.0), 290 (−8.6), 310 (+7.4) nm.

Compound **19b:** ECD (*c* 2.0 mM, CH_3CN) λ_{max} (Δε) 190 (+28.1), 202 (+12.9), 216 (+20.0), 232 (−14.9), 249 (−2.1), 266 (−6.0), 292 (+8.4), 310 (−7.2) nm.

Compound **23**: yellowish, amorphous solid; insufficient material available for optical rotation; HPLC-UV (MeOH in H_2O + 0.1% FA) λ_{max} 208, 219, 296-326 nm; ^{1}H and ^{13}C NMR data, see Tables 2 and 3; (+)HRESIMS *m/z* [M + H]$^+$ calcd for $C_{20}H_{23}O_3^+$, 311.1642, found 311.1641, ΔM +0.2 ppm; [M + Na]$^+$ calcd for $C_{20}H_{22}O_3Na^+$, 333.1461, found 333.1446, ΔM +4.5 ppm.

Compound **23a:** ECD (*c* 3.2 mM, CH_3CN) λ_{max} (Δε) 190 (−5.5), 213 (+6.1), 244 (+1.7), 261 (−0.3), 311 (−0.7) nm.

Compound **23b:** ECD (*c* 2.4 mM, CH_3CN) λ_{max} (Δε) 190 (+5.7), 213 (−5.1), 244 (−1.1), 258 (+0.4), 311 (+0.7) nm.

Compound **24**: yellowish, amorphous solid; insufficient material available for optical rotation; HPLC-UV (MeOH in H_2O + 0.1% FA) λ_{max} 201, 225, 278–292 nm; ^1H and ^{13}C NMR data, see Tables 2 and 3; (+)HRESIMS *m/z* $[M + H]^+$ calcd for $C_{30}H_{29}O_6^+$, 485.1959, found 485.1943, ΔM +3.2 ppm; $[M + Na]^+$ calcd for $C_{30}H_{28}O_6Na^+$, 507.1778, found 507.1760, ΔM +3.6 ppm.

Compound **24a:** ECD (*c* 2.0 mM, CH_3CN) λ_{max} (Δε) 190 (−25.0), 204 (+14.7), 216 (+24.3), 233 (−29.3), 260 (−0.6), 280 (+9.5), 306 (−31.1) nm.

Compound **24b:** ECD (*c* 3.1 mM, CH_3CN) λ_{max} (Δε) 190 (+26.7), 204 (−13.5), 216 (−23.4), 233 (+30.1), 260 (+1.4), 280 (−8.5), 306 (+32.0) nm.

Compound **25**: yellowish, amorphous solid; insufficient material available for optical rotation; HPLC-UV (MeOH in H_2O + 01% FA) λ_{max} 206, 222, 278–292 nm; ^1H and ^{13}C NMR data, see Tables 2 and 3; (+)HRESIMS *m/z* $[M + H]^+$ calcd for $C_{30}H_{29}O_6^+$, 485.1959, found 485.1943, ΔM +3.2 ppm; $[M + Na]^+$ calcd for $C_{30}H_{28}O_6Na^+$, 507.1778, found 507.1760, ΔM +3.6 ppm.

Compound **25a:** ECD (*c* 2.0 mM, CH_3CN) λ_{max} (Δε) 190 (+6.4), 203 (+17.6), 212 (−18.1), 223 (+4.7), 238 (+3.5), 274 (−6.0), 307 (+4.6) nm.

Compound **25b:** ECD (*c* 1.8 mM, CH_3CN) λ_{max} (Δε) 190 (−6.0), 203 (−16.9), 212 (+18.3), 223 (−4.3), 238 (−3.1), 274 (+6.1), 307 (−4.4) nm.

3.7. ECD Data Acquisition and Calculations

ECD spectra were recorded on a J-1500 spectrometer (JASCO, Tokyo, Japan) equipped with a 1 mm path length cuvette. Calculation of ECD spectra was performed essentially as suggested for good computational practice for assignment of absolute configuration by comparison of calculated and experimental ECD spectra [46]. Thus, after establishment of the relative configuration by NMR spectroscopy, conformational searches for **6a**, **11b**, **14b**, **15b**, **17a**, **18b**, **19a**, **23b**, **24a** and **25b** were performed with MacroModel in Maestro ver. 11.8 (Schrödinger, New York, NY, USA) in the gas phase (energy window 21 kJ/mol) using Molecular Merck force field *static* (MMFFs). This yielded one conformer for **15b**, **17a**, **18b**, **19a**, **24a** and **25b**; two conformers for **11b**, **14b** and **23b**; and ten conformers for compound **6a** (Boltzmann's population fraction weight threshold >0.5%, see supplementary information). The geometries of the selected conformers were optimized using density functional theory (DFT) with B3LYP/6-31G(d,p) level of theory in CH_3CN [47,48] adopting to the polarizable continuum model (PCM) to describe the solvent [49,50]. Subsequently, the ECD spectra of each conformer were calculated with time-dependent density functional theory (TDDFT) at the B3LYP/6-311G(d,p) level in CH_3CN solution as described by PCM [51]. 20 excited states of each conformer were included for **6a**, **11b**, **14b**, **15b**, **17a** and **23b**, 30 excited states of each conformer were included for **18b**, **24a** and **25b**, and 40 excited states of each conformer were included for **19a**. All DFT and TDDFT calculations were performed using the Gaussian16 package [52] (Gaussian, Inc., Wallingford, CT, USA) with Gaussian's default setup for the PCM calculations. The final calculated ECD spectrum of each compound was generated by averaging the individual spectra of its low-energy conformer according to their Boltzmann distribution using SpecDis23 ver. 1.71 (Berlin, Germany) [53] adopting the following bandwidths and UV shifts: **6a**: 0.18 eV, −4 nm, **11b**: 0.30 eV, −1 nm, **14b**: 0.20 eV, −4 nm, **15b**: 0.30 eV, 4 nm, **17a**: 0.30 eV, −3 nm, **18b**: 0.28 eV, 2 nm, **19a**: 0.20 eV, 2 nm, **23b**: 0.20 eV, −1 nm, **24a**: 0.28 eV, 8 nm, and **25b**: 0.20 eV, 1 nm. Calculated and experimental ECD spectra were compared quantitatively by calculation of the enantiomeric similarity index (Δ_{ESI}) [53] using built-in routines in SpecDisc. Geometry optimization and calculation of ECD spectra were also attempted with CAM-B3LYP in combination with e.g., the 6-311G(d,p) and/or aug-cc-pvdz basis sets, but resulted in less reliable data.

3.8. NMR Experiments

NMR experiments were recorded with standard pulse programs on 600 MHz Avance III spectrometers (Bruker BioSpin, Karlsruhe, Germany) equipped with 1.7-mm TCI and 5-mm DCH cryoprobes using 1.7- or 2.5-mm NMR tubes, respectively. Samples were recorded in methanol-d_4 at 300 K, and ^{1}H and ^{13}C NMR chemical shifts were referenced to the residual solvent signal of methanol-d_4 (δ 3.31 and δ 49.0, respectively). ^{1}H NMR spectra were recorded using 30° pulses and 64 k data points. For the 2D NMR experiments, phase-sensitive DQF-COSY and ROESY spectra were recorded using a gradient-based pulse sequence with 12 ppm spectral width and 2k × 512 data points (processed with forward linear prediction to 1k data points in F1); a multiplicity-edited HSQC spectrum was acquired with the following parameters: $^1J_{C,H}$ = 145 Hz, spectral width 12 ppm for ^{1}H and 170 ppm for ^{13}C, 1730 × 256 data points (processed with both forward linear prediction and zero filling to 1k data points in F1), and 1.0 s relaxation delay; HMBC experiment was optimized for $^nJ_{C,H}$ = 8.0 Hz (long range), $^1J_{C,H\,min}$ = 125 Hz, $^1J_{C,H\,max}$ = 160 Hz and acquired using a spectral width of 12 ppm for ^{1}H and 240 ppm for ^{13}C, 2k × 256 data points (processed with forward linear prediction to 512 data points and zero filling to 1k data points in F1), and a 1.0 s relaxation delay.

3.9. X-ray Crystallographic Analysis of 19

Single crystals suitable for X-ray diffraction studies were grown in deuterated methanol. A single crystal was mounted and immersed in a stream of nitrogen gas [T = 123(2) K]. Data were collected, using graphite-monochromated CuKα radiation (λ = 1.54178 Å) on a Bruker D8 Venture diffractometer. Data collection and cell refinement were performed using the Bruker Apex2 Suite software (Bruker AXS, Madison, WI, USA). Data reduction using SAINT ver. 8.37A (Bruker AXS) and multi-scan correction for absorption using Bruker/Siemens Area Detector Absorption Correction program SADABS-2016-2 (Bruker/Siemens Area Detector Absorption Correction program) were performed within the Apex2 Suite. The crystal data, data collection and the refinement data are given in Supplementary Material Table S16.

Positions of all non-hydrogen atoms were found by direct methods (SHELXS97) [54]. Full-matrix least-squares refinements (SHELXL-2018/3) [55] were performed on F^2, minimizing $\Sigma w(F_o^2 - kF_c^2)^2$, with anisotropic displacement parameters of the non-hydrogen atoms. The positions of hydrogen atoms were located in subsequent difference electron density maps and were included in calculated position with fixed isotropic displacement parameters ($Uiso$ = 1.2Ueq for CH, and $Uiso$ = 1.5Ueq for CH_3). Refinement (space group $C2/c$: 374 parameters, 5191 unique reflections) converged at R_F = 0.0357, wRF^2 = 0.0868 [4591 reflections with Fo > 4σ(F_o); $w^{-1} = (\sigma^2(F_o^2) + (0.0381P)^2 + 5.584P)$, where $P = (F_o^2 + 2F_c^2)/3$; S = 1.037]. The residual electron density varied between -0.33 and 0.35 e Å^{-3}. Complex scattering factors for neutral atoms were taken from International Tables for Crystallography as incorporated in SHELXL [55,56]. Fractional atomic coordinates, a list of anisotropic displacement parameters, and a complete list of geometrical data has been deposited in the Cambridge Crystallographic Data Centre (CCDC 1982785). Copies of the data can be obtained, free of charge, on application to the director, CCDC, 12 Union Road, Cambridge CB2 1EZ, UK (fax: +44 1223 336 033 or e-mail: deposit@ccdc.cam.ac.uk).

4. Conclusions

To summarize, 13 new prenyl- and geranyl-substituted coumarin derivatives were isolated and identified in the ethyl acetate extract of *G. piloselloides*, guided by combined use of HPLC-PDA-HRMS and dual high-resolution PTP1B/α-glucosidase inhibition profiling for pinpointing new natural products as inhibitors of PTP1B and/or α-glucosidase. Compound **6** with a furan-oxepane 5/7 ring system represents a novel class of geranyl-substituted coumarin, and compounds **19** and **24** also represent a novel class of dimeric natural products consisting of both coumarin and chromone moieties. Interestingly, chiral resolution showed that ten of the compounds were racemic mixtures, and the absolute configuration of the separated enantiomers **6a/b**, **11a/b**, **14a/b**, **15a/b**, **17a/b**, **18a/b**, **19a/b**, **23a/b**, **24a/b** and **25a/b** were determined by comparison of their experimental and calculated ECD spectra

as well as by single X-ray crystallography of one of the isolated dimeric coumarin derivatives (**19**). This study demonstrates the advantage of the combined use of dual high-resolution inhibition profiling and hyphenated LC-PDA-HRMS for pinpointing new compounds with potential as dual inhibitors, and the microplate-based inhibition profiling can be extended to include multiple pharmacological targets. Further improvement in the preparative-scale chiral separation of enantiomers is however needed to allow isolation of enantiomerically pure material for further characterization of the mode of inhibition.

Supplementary Materials: The following are available online, HRMS and 1D data of known compounds, chromatograms from chiral separations, ECD spectra, details of ECD calculation, X-ray crystallographic analysis of **19**, and 1D and 2D NMR spectra of new compounds identified in this study.

Author Contributions: Conceptualization, T.L., K.F., S.C., P.R.H., K.T.K., D.S.; Formal analysis, T.L., D.F., L.K.; K.F., S.C., D.S.; Funding acquisition, T.L., S.C.; Investigation, T.L., X.M., L.K.; Project administration, D.S.; Supervision, S.C., P.R.H., K.T.K., D.S.; Visualization, T.L., D.F., K.F., D.S.; Writing—original draft, T.L., K.F., S.C., D.S.; Writing—review & editing, T.L., X.M., D.F., L.K., K.F., P.R.H., K.T.K., D.S. All authors have read and agreed to the published version of the manuscript.

Funding: Tuo Li acknowledges the Chinese Scholarship Council for a scholarship (No. 201508530232). HPLC equipment used for high-resolution inhibition profiling was obtained via a grant from The Carlsberg Foundation. Daniil Fedotov and Sonia Coriani acknowledge support from the Marie Sklodowska-Curie European Training Network "COSINE-COmputational Spectroscopy In Natural sciences and Engineering", Grant Agreement No. 765739.

Acknowledgments: Arife Önder is gratefully thanked for technical assistance, and Niels Vissing Holst, Department of Chemistry, University of Copenhagen, is gratefully acknowledged for collection of X-ray data and data reduction.

Conflicts of Interest: The authors declare no conflict of interest.

References

1. International Diabetes Federation. *IDF Diabetes Atlas*, 9th ed.; International Diabetes Federation: Brussels, Belgium, 2019; ISBN 978-2-930229-87-4. Available online: http://www.diabetesatlas.org/ (accessed on 4 April 2020).
2. Chatterjee, S.; Khunti, K.; Davies, M.J. Type 2 diabetes. *Lancet* **2017**, *389*, 2239–2251. [CrossRef]
3. Marcovecchio, M.L.; Lucantoni, M.; Chiarelli, F. Role of chronic and acute hyperglycemia in the development of diabetes complications. *Diabetes Technol. Ther.* **2011**, *13*, 389–394. [CrossRef]
4. Zhang, S.; Zhang, Z.Y. PTP1B as a drug target: Recent developments in PTP1B inhibitor discovery. *Drug Discov. Today* **2007**, *12*, 373–381. [CrossRef] [PubMed]
5. Abdelsalam, S.S.; Korashy, H.M.; Zeidan, A.; Agouni, A. The role of protein tyrosine phosphatase (PTP)-1B in cardiovascular disease and its interplay with insulin resistance. *Biomolecules* **2019**, *9*, 286. [CrossRef]
6. He, Z.X.; Zhou, Z.W.; Yang, Y.; Yang, T.; Pan, S.Y.; Qiu, J.X.; Zhou, S.F. Overview of clinically approved oral antidiabetic agents for the treatment of type 2 diabetes mellitus. *Clin. Exp. Pharm. Physiol* **2015**, *42*, 125–138. [CrossRef] [PubMed]
7. Derosa, G.; Maffioli, P. α-Glucosidase inhibitors and their use in clinical practice. *Arch. Med. Sci.* **2012**, *8*, 899–906. [CrossRef] [PubMed]
8. Jiangsu New Medical College. *Dictionary of Traditional Chinese Medicine*; Shanghai Science and Technology Publishing House: Shanghai, China, 1977; Volume 114, pp. 1009–1423.
9. Nagumo, S.; Takao Inoue, K.I.; Nagai, M. Cyanogenic glycosides and 4-hydroxycoumarin glycosides from *Gerbera jamesonii* hybrida. *Chem. Pharm. Bull.* **1985**, *33*, 4803–4806. [CrossRef]
10. Nagumo, S.; Takao Inoue, T.T.; Nagai, M. New glucosides of a 4-hydroxy-5-methylcoumarin and a dihydro-α-pyrone from *Gerbera jamesonii* hybrida. *Chem. Pharm. Bull.* **1989**, *37*, 2621–2623. [CrossRef]
11. Xiao, Y.; Ding, Y.; Li, J.B.; Nohara, T. Two novel dicoumaro-*p*-menthanes from *Gerbera piloselloides* (L.) CASS. *Chem. Pharm. Bull.* **2004**, *52*, 1362–1364. [CrossRef]
12. Liu, S.Z.; Feng, J.-Q.; Wu, J.; Zhao, W.M. A new monoterpene-coumarin and a new monoterpene-chromone from *Gerbera delavayi*. Helv. *Chim. Acta* **2010**, *93*, 2026–2029. [CrossRef]
13. Qiang, Y.; Chen, Y.J.; Li, Y.; Zhao, J.; Gao, K. Coumarin derivatives from *Gerbera saxatilis*. *Planta Med.* **2011**, *77*, 175–178. [CrossRef] [PubMed]

14. He, F.; Wang, M.; Gao, M.; Zhao, M.; Bai, Y.; Zhao, C. Chemical composition and biological activities of *Gerbera anandria*. *Molecules* **2014**, *19*, 4046–4057. [CrossRef] [PubMed]
15. Wang, J.; Petrova, V.; Wu, S.B.; Zhu, M.; Kennelly, E.J.; Long, C. Antioxidants from *Gerbera piloselloides*: An ethnomedicinal plant from southwestern China. *Nat. Prod. Res.* **2014**, *28*, 2072–2075. [CrossRef] [PubMed]
16. Brahmachari, G.; Da, S.; Kumar, A.; Misra, N.; Sharma, S.; Gupta, V.K. Structural confirmation, single X-ray crystallographic behavior, molecular docking and other physico-chemical properties of gerberinol, a natural dimethyl dicoumarol from *Gerbera lanuginosa* Benth. (Compositae). *J. Mol. Struct.* **2017**, *1136*, 214–221. [CrossRef]
17. Cesar, G.Z.; Alfonso, M.G.; Marius, M.M.; Elizabeth, E.M.; Angel, C.B.; Maira, H.R.; Guadalupe, C.L.; Manuel, J.E.; Ricardo, R.C. Inhibition of HIV-1 reverse transcriptase, toxicological and chemical profile of *Calophyllum brasiliense* extracts from Chiapas, Mexico. *Fitoterapia* **2011**, *82*, 1027–1034. [CrossRef] [PubMed]
18. Ali, M.Y.; Jannat, S.; Jung, H.A.; Jeong, H.O.; Chung, H.Y.; Choi, J.S. Coumarins from *Angelica decursiva* inhibit alpha-glucosidase activity and protein tyrosine phosphatase 1B. *Chem. Biol. Interact* **2016**, *252*, 93–101. [CrossRef]
19. Bohlmann, F.; Grenz, M. Natürlich vorkommende cumarin-derivate, XI. Über die inhaltsstoffe von *Gerbera piloselloides* Cass. *Chem. Ber.* **1975**, *108*, 26–30. [CrossRef]
20. Schmidt, J.S.; Lauridsen, M.B.; Dragsted, L.O.; Nielsen, J.; Staerk, D. Development of a bioassay-coupled HPLC-SPE-ttNMR platform for identification of α-glucosidase inhibitors in apple peel (*Malus* × *domestica* Borkh.). *Food Chem.* **2012**, *135*, 1692–1699. [CrossRef]
21. Okutan, L.; Kongstad, K.T.; Jäger, A.K.; Staerk, D. High-resolution α-amylase assay combined with high-performance liquid chromatography–solid-phase extraction–nuclear magnetic resonance spectroscopy for expedited identification of α-amylase inhibitors: Proof of concept and α-amylase inhibitor in cinnamon. *J. Agric. Food Chem.* **2014**, *62*, 11465–11471. [CrossRef]
22. Tahtah, Y.; Kongstad, K.T.; Wubshet, S.G.; Nyberg, N.T.; Jønsson, L.H.; Jäger, A.K.; Qinglei, S.; Staerk, D. Triple aldose reductase/α-glucosidase/radical scavenging high-resolution profiling combined with high-performance liquid chromatography–high-resolution mass spectrometry–solid-phase extraction–nuclear magnetic resonance spectroscopy for identification of antidiabetic constituents in crude extract of Radix Scutellariae. *J. Chromatogr. A* **2015**, *1408*, 125–132.
23. Tahtah, Y.; Wubshet, S.G.; Kongstad, K.T.; Heskes, A.M.; Pateraki, I.; Møller, B.M.; Jäger, A.K.; Staerk, D. High-resolution PTP1B inhibition profiling combined with high-performance liquid chromatography-high-resolution mass spectrometry-solid-phase extraction-nuclear magnetic resonance spectroscopy: Antidiabetic constituents in crude extract of *Eremophila lucida*. *Fitoterapia* **2016**, *110*, 52–58. [PubMed]
24. Wiese, S.; Wubshet, S.G.; Nielsen, J.; Staerk, D. Coupling HPLC-SPE-NMR with a microplate-based high-resolution antioxidant assay for efficient analysis of antioxidants in food – Validation and proof-of-concept study with caper buds. *Food Chem.* **2013**, *141*, 4010–4018. [CrossRef] [PubMed]
25. Li, T.; Kongstad, K.T.; Staerk, D. Identification of α-glucosidase inhibitors in *Machilus litseifolia* by combined use of high-resolution α-glucosidase inhibition profiling and HPLC-PDA-HRMS-SPE-NMR. *J. Nat. Prod.* **2019**, *82*, 249–258. [CrossRef] [PubMed]
26. Lima, R.C.L.; Kato, L.; Kongstad, K.T.; Staerk, D. Brazilian insulin plant as a bifunctional food: Dual high-resolution PTP1B and α-glucosidase inhibition profiling combined with HPLC-HRMS-SPE-NMR for identification of antidiabetic compounds in *Myrcia rubella* Cambess. *J. Funct. Food* **2018**, *45*, 444–451. [CrossRef]
27. Zhao, Y.; Kongstad, K.T.; Jäger, A.K.; Nielsen, J.; Staerk, D. Quadruple high-resolution α-glucosidase/α-amylase/PTP1B/radical scavenging profiling combined with high-performance liquid chromatography-high-resolution mass spectrometry-solid-phase extraction-nuclear magnetic resonance spectroscopy for identification of antidiabetic constituents in crude root bark of *Morus alba* L. *J. Chromatogr. A* **2018**, *1556*, 55–63. [PubMed]
28. Trumble, J.T.; Millar, J.G. Biological activity of marmesin and demethylsuberosin against a generalist herbivore, *Spodoptera exigua* (Lepidoptera: Noctuidae). *J. Agric. Food Chem.* **1996**, *44*, 2859–2864. [CrossRef]
29. Chen, Y.J.; Li, Y.; Chen, J.J.; Gao, K. Benzofuran derivatives from *Gerbera saxatilis*. *Helv. Chim. Acta* **2007**, *90*, 176–182. [CrossRef]

30. Garc, S.K.; Gupta, S.R.; Sharma, N.D. Coumarins from *Apium graveolens* seeds. *Phytochemistry* **1979**, *18*, 1580–1581. [CrossRef]
31. Appendino, G.; Cravotto, G.; Giovenzana, G.B.; Palmisano, G. A straightforward entry into polyketide monoprenylated furanocoumarins and pyranocoumarins. *J. Nat. Prod.* **1999**, *62*, 1627–1631. [CrossRef]
32. Bohlmann, F.; Zdero, C.; Frunke, H. Uber die inhaltsstoffe der gattung *Gerbera*. *Chem. Ber.* **1973**, *106*, 382–387. [CrossRef]
33. Bohlmann, F.; Grenz, M. Uber die inhaltsstoffe der gattung *Flourensia*. *Chem. Ber.* **1977**, *110*, 295–300. [CrossRef]
34. Viturro, C.I.; Fuente, J.R.; Maier, M.S. Antifungal methylphenone derivatives and 5-methylcoumarins from *Mutisia friesiana*. *Z. Nat. C* **2003**, *58*, 533–540. [CrossRef] [PubMed]
35. Lou, H.X.; Sun, L.R.; Yu, W.T.; Fan, P.H.; Cui, L.; Gao, Y.H.; Ma, B.; Ren, D.M.; Ji, M. Absolute configuration determination of angular dihydrocoumarins from *Peucedanum praeruptorum*. *J. Asian Nat. Prod. Res.* **2004**, *6*, 177–184. [CrossRef] [PubMed]
36. Bohlmann, F.; Zdero, C.; Le Van, N. Neue geranyl-cumarin-derivate und weitere inhaltsstoffe aus der tribus Mutisieae. *Phytochemistry* **1979**, *18*, 99–102. [CrossRef]
37. Marzocco, S.; Adesso, S.; Alilou, M.; Stuppner, H.; Schwaiger, S. Anti-inflammatory and anti-oxidant potential of the root extract and constituents of *Doronicum austriacum*. *Molecules* **2017**, *22*, 1003. [CrossRef]
38. Shanmugasundaram, M.; Manikandan, S.; Raghunathan, R. High chemoselectivity in microwave accelerated intramolecular domino Knoevenagel hetero Diels-Alder reactions—An efficient synthesis of pyrano[3-2c]coumarin framework. *Tetrahedron* **2002**, *58*, 997–1003. [CrossRef]
39. Farrugia, L.J. ORTEP-3 for Windows—A version of ORTEP-III with a graphical user interface (GUI). *J. Appl. Crystallogr.* **1997**, *30*, 565. [CrossRef]
40. Rashid, M.A.; Armstrong, J.A.; Gray, A.I.; Waterman, P.G. Tetra- and pentacyclic 6-C-monoterpenyl-5,7-dioxycoumarins from *Eriostemon brucei* and *E. brucei* subspecies *cinereus*. *Phytochemistry* **1992**, *31*, 3583–3588. [CrossRef]
41. Huang, G.H.; Hu, Z.; Lei, C.; Wang, P.P.; Yang, J.; Li, J.Y.; Li, J.; Hou, A.J. Enantiomeric pairs of meroterpenoids with diverse heterocyclic systems from Rhododendron nyingchiense. *J. Nat. Prod.* **2018**, *81*, 1810–1818. [CrossRef]
42. Pietiainen, M.; Kontturi, J.; Paasela, T.; Deng, X.B.; Ainasoja, M.; Nyberg, P.; Hotti, H.; Teeri, T.H. Two polyketide synthases are necessary for 4-hydroxy-5-methylcoumarin biosynthesis in *Gerbera hybrida*. *Plant J.* **2016**, *87*, 548–558. [CrossRef]
43. Shoyama, Y.; Takeuchi, A.; Taura, F.; Tamada, T.; Adachi, M.; Kuroki, R.; Shoyama, Y.; Morimoto, S. Crystallization of Delta1-tetrahydrocannabinolic acid (THCA) synthase from Cannabis sativa. *Acta Cryst. Sect. F Struct. Biol. Cryst. Commun.* **2005**, *61*, 799–801. [CrossRef] [PubMed]
44. Li, H.; Tang, Y.; Hsung, R.P. Investigating thermal dimerization of *N*-methyl-flindersine. Syntheses and characterizations of paraensidimerines. *Tetrahedron Lett.* **2012**, *53*, 6138–6143. [CrossRef]
45. Wubshet, S.G.; Tahtah, Y.; Heskes, A.M.; Kongstad, K.T.; Pateraki, I.; Hamberger, B.; Møller, B.M.; Staerk, D. Identification of PTP1B and α-glucosidase inhibitory serrulatanes from *Eremophila* spp. by combined use of dual high-resolution PTP1B and α-glucosidase inhibition profiling and HPLC-HRMS-SPE-NMR. *J. Nat. Prod.* **2016**, *79*, 1063–1072. [CrossRef] [PubMed]
46. Pescitelli, G.; Bruhn, T. Good computational practice in the assignment of absolute configurations by TDDFT calculations of ECD spectra. *Chirality* **2016**, *28*, 466–474. [CrossRef] [PubMed]
47. Becke, A.D. Density-functional thermochemistry. III. The role of exact exchange. *J. Chem. Phys.* **1993**, *98*, 5648–5652. [CrossRef]
48. Stephens, P.J.; Devlin, F.J.; Chabalowski, C.F.; Frisch, M.J. Ab initio calculation of vibrational absorption and circular dichroism spectra using density functional force fields. *J. Phys. Chem.* **1994**, *98*, 11623–11627. [CrossRef]
49. Miertuš, S.; Scrocco, E.; Tomasi, J. Electrostatic interaction of a solute with a continuum. A direct utilizaion of ab-initio molecular potentials for the prevision of solvent effects. *Chem. Phys.* **1981**, *55*, 117–129. [CrossRef]
50. Tomasi, J.; Mennucci, B.; Cammi, R. Quantum mechanical continuum solvation models. *Chem. Rev.* **2005**, *105*, 2999–3093. [CrossRef]
51. Warnke, I.; Furche, F. Circular dichroism: Electronic. *Wires Comput. Mol. Sci.* **2012**, *2*, 150–166. [CrossRef]

52. Frisch, M.J.; Trucks, G.W.; Schlegel, H.B.; Scuseria, G.E.; Robb, M.A.; Cheeseman, J.R.; Scalmani, G.; Barone, V.; Petersson, G.A.; Nakatsuji, H.; et al. *Gaussian 16 Rev. B.01*; Gaussian Inc.: Wallingford, CT, USA, 2016.
53. Bruhn, T.; Schaumloffel, A.; Hemberger, Y.; Bringmann, G. SpecDis: Quantifying the comparison of calculated and experimental electronic circular dichroism spectra. *Chirality* **2013**, *25*, 243–249. [CrossRef]
54. Sheldrick, G.M. A short history of SHELX. *Acta Crystallogr. Sect. A Found. Adv.* **2008**, *64*, 112–122. [CrossRef] [PubMed]
55. Sheldrick, G.M. Crystal structure refinement with SHELXL. *Acta Crystallogr. Sect. C Struct. Chem.* **2015**, *71*, 3–8. [CrossRef] [PubMed]
56. *International Tables for Crystallography*; Wilson, A.J.C. (Ed.) Kluwer Academic Publishers: Dordrecht, The Netherlands, 1995; Volume C.

Sample Availability: Not available.

© 2020 by the authors. Licensee MDPI, Basel, Switzerland. This article is an open access article distributed under the terms and conditions of the Creative Commons Attribution (CC BY) license (http://creativecommons.org/licenses/by/4.0/).